Optical properties of $A_2^{IV}B_2^{V}C_6^{VI}$ ferroelectrics-semiconductors: the effect of temperature and hydrostatic pressure

Review

Gerzanich E. I.

Uzhgorod National University, 52 Voloshyn St., 88000 Uzhgorod, Ukraine

Abstract

In this review the results of experimental studies for the influence of temperature and high pressure on the fundamental absorption edge, optical birefringence and vibrational spectra of $A_2^{IV}B_2^{V}C_6^{VI}$ -group crystals are presented. It is revealed that the high-energy part of the absorption edge is described by the Urbach rule, while its low-energy part is formed by indirect optical transitions. Violation of the Urbach rule is detected in the region of incommensurate phase. The temperature and baric coefficients of the forbidden gap in the ferroelectric, paraelectric and incommensurate phases are found to be negative. Electron-phonon interaction plays a major part in the temperature changes of the bandgap. According to the theory, the bandgap suffers characteristic anomalies that depend upon the phase transition order. The critical indices of the order parameter and heat capacity and the Landau-Ginzburg expansion coefficients derived from the baric studies of optical birefringence agree well with a presence of Lifshitz point at the p,T-diagrams of the crystals under test. Relative shift in the frequencies of the Raman spectra occurring under mechanical stresses testifies a notable nonequivalence of atomic bonds and a possibility of dividing the vibrations in $Sn_2P_2S_6$ into the external and internal ones. The results of baric investigations of the Raman spectra show that the structural transformation in $Sn_2P_2S_6$ is mainly linked to Sn-S bonds. The results analysed by us testify a possibility for practical applications of $Sn_2P_2S_6$ ferroelectrics as a converter of coherent long-wave radiation into shorter-wave one.

1. Introduction

Crystals of $A_2^{IV}B_2^{V}C_6^{VI}$ family represent a proper uniaxial ferroelectric [1]. At the room temperature $Sn_2P_2S_6$ has the acentric structure *Pc* of monoclinic syngony, while $Sn_2P_2Se_6$, $Pb_2P_2S_6$ and $Pb_2P_2Se_6$ are described by the acentric space group $P2_1/c$. When the temperature of $Sn_2P_2S_6$ increases, a second-order phase transition occurs at $T = T_0 = 339\,\text{K}$, giving rise to a paraelectric state. The space group is then changed from

Pc to $P2_1/c$ [2]. The ferroelectrics of $A_2^{IV}B_2^{V}C_6^{VI}$ family are isostructural and manifest ionic-covalent bonding, thus favouring existence of a continuous row of solid solutions $(Pb_ySn_{1-y})_2P_2(Se_xS_{1-x})_6$ [3–5]. When the ions constituting $Sn_2P_2S_6$ and the solid solutions on its basis are isomorphously substituted or the external hydrostatic pressure increases, the T_0 temperature decreases. Moreover, in this case a so-called Lifshitz point and an incommensurate phase appear on the $p,T,x(y)$-diagram. The period of the modulated wave of atomic displacements in the incommensurate phase is 12–14 times greater that the lattice constants of the basic structure [6]. The three phases coincide at the Lifshitz point, the high-temperature paraelectric phase, low-temperature ferroelectric one and the incommensurate phase. We employ the following notation for characterizing the phase transitions: T_0 is the second-order paraelectric-to-ferroelectric phase transition, T_i the second-order paraelectric-to-incommensurate phase transition and, finally, T_c the point of the first-order incommensurate-to-ferroelectric phase transition.

Under increasing hydrostatic pressure, the p,T-diagram of $Sn_2P_2S_6$ exhibits the Lifshitz point at $T = 295\,\text{K}$ and $p = p_L = 0.19\,\text{GPa}$. Further increase in pressure leads to splitting of the phase transition line $T_0(p)$ into two lines corresponding to the phase transitions $T_i(p)$ and $T_c(p)$. The incommensurate phase exists between the lines mentioned above in the p,T-plane, the region of the latter being widened with increasing p. The baric coefficients for the points T_0, T_i and T_c are respectively $\dfrac{dT_0}{dp} = -220$,

$\dfrac{dT_i}{dp} = -216$ and $\dfrac{dT_c}{dp} = -238\,\dfrac{\text{K}}{\text{GPa}}$.

The x,T-diagrams for the solid solutions $Sn_2P_2(Se_xS_{1-x})_6$ show the same effects, including the appearance of the Lifshitz point and the incommensurate phase. In particular, the Lifshitz point appears on the x,T-diagram at $x = x_L = 0.28$ and $p = p_{atm}$, whereas at $x > x_L$ the phase transition line $T_0(x)$ is split into the two lines $T_i(x)$ and $T_c(x)$, with additional existence of the incommensurate phase. Then the increase in x causes broadening of the region of incommensurate phase.

Hence, the incommensurate phase in $Sn_2P_2Se_6$ crystals is available in the temperature range $\Delta T = T_i - T_c$ (where $T_i = 222\,\text{K}$ and $T_c = 193\text{K}$) already at $p = p_{atm}$. The baric coefficients for T_i and T_c are equal to $\dfrac{dT_i}{dp} = -163\,\dfrac{\text{K}}{\text{GPa}}$ and $\dfrac{dT_c}{dp} = -245\,\dfrac{\text{K}}{\text{GPa}}$, respectively.

Isomorphous substitution of Sn for Pb in the solid $(Pb_ySn_{1-y})_2P_2S_6$ solutions at $p = p_{atm}$ gives rise to lower T_0, which becomes as low as 4.2K at $y = 0.61$. Nonetheless, character of the phase transition remains the same [6, 8]. Hydrostatic pressure decreases the T_0 value and the p,T-diagrams reveal the Lifshitz point. In this

case the Lifshitz point is shifted towards higher pressures with increasing y. Thus, replacement of S with Se in the solid solutions $Sn_2P_2(Se_xS_{1-x})_6$ draws the phase transitions to the Lifshitz point, while for the $(Pb_ySn_{1-y})_2P_2S_6$ system we have a contrary situation, i.e. the phase transitions move away from the Lifshitz point with increasing Pb content.

Substitution of Sn with Pb in the solid solutions $(Pb_ySn_{1-y})_2P_2Se_6$ decreases the T_i and T_c values. The temperature region where the incommensurate phase exists broadens out; it is larger than 100 K at $y = 0.4$. This broadening is accompanied by increasing temperature hysteresis of the phase transition at T_c [6, 9]. At $T = 4.2\,K$ the incommensurate phase appears in the y region limited by 0.40 and 0.64.

The phase diagrams for the $Sn_2P_2S_6$-family crystals described above testify that the compounds under test belong to ferroelectrics of a displacement type. They show that replacements of isomorphous ions in the solid solutions based on $Sn_2P_2S_6$ turn out to be analogous to the effect of hydrostatic pressure. The Lifshitz points and the incommensurate phase occur on the $p,T,x(y)$-diagrams, which have been observed for the first time on the example of $A_2^{IV}B_2^{V}C_6^{VI}$-group crystals.

Furthermore, the crystals under study possess semiconducting properties. The latter fact essentially extends the methods of their theoretical and experimental investigations and, moreover, offers various applications. Naturally, the main features of the phase diagrams affect the optical properties of those ferroelectrics-semiconductors, in particular the absorption of light, optical birefringence and the vibrational spectra.

Fundamental absorption edge is the most typical feature of optical properties of a semiconductor. The structure of the absorption edge reflects the structure of the valence and conduction bands in the region of electron quasi-momenta where the bands are close to each other. Ferroelectrics-semiconductors also manifest anomalous behaviour of the absorption edge in the course of phase transitions. Studies of optical birefringence in the vicinity of phase transitions along the p,T-diagram enable one to determine the critical indices of those transitions and the Landau-Ginzburg coefficients in the expansion of thermodynamic potential. This knowledge should allow comparing the experimental results to the theory of phase transitions. Studies of the Raman spectra of ferroelectrics under external pressure provides valuable information on anharmonicity of the lattice vibrations and the vibrational spectra in the conditions when the interatomic distances are modified, the chemical content invariable and the population of energy levels in crystals is temperature-dependent.

Thus, experimental measurements of the absorption edge, birefringence and the vibrational spectra under influence of temperature and hydrostatic pressure enable researchers to get information concerning the peculiarities of light absorption, the energy structure, character of the phase transitions, critical phenomena and the vibrational spectra of ferroelectrics-semiconductors in the regions of both commensurate and incommensurate phases and in the vicinity of phase transitions.

2. Fundamental absorption edge and the Urbach rule

The absorption edge of $Sn_2P_2S_6$ has been investigated for the first time in the work [4]. It has been revealed that the edge corresponds to $\lambda=530$ nm at the atmospheric pressure and $T=295$ K, whereas at $T=77$ K one has the value $\lambda=497$ nm. The energy position of the absorption edge $E_g^\alpha = h\nu_\alpha$ (with α being the absorption coefficient) for $Sn_2P_2S_6$ and its structural analogs is shown in Fig. 1. It is seen that the substitution $S \rightarrow Se$ in the anion sublattice decreases the E_g^α value, while the substitution $Sn \rightarrow Pb$ produces the contrary effect [10].
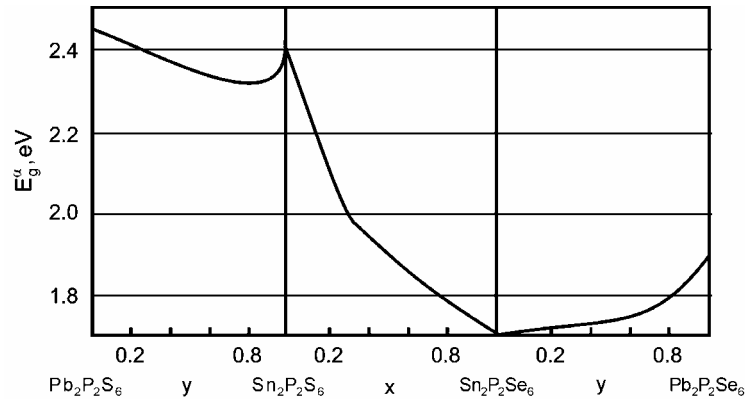
Fig. 1. Concentration dependences of E_g^α $\left(\alpha=150\,cm^{-1}\right)$ for the solid solutions based on $Sn_2P_2S_6$ at $T=293$ K and $p=p_{atm}$ [10].

The shape of the absorption edge is an important characteristic. For the case of $Sn_2P_2S_6$ crystals and their analogs it has been studied in the works [11–17]. In particular, it has been demonstrated in Ref. [11, 12] that the low-energy part of the absorption edge for $Sn_2P_2S_6$ reveals peculiarities typical for the crystals with indirect optical transitions. Later on, the structure of energy bands has been calculated, thus evidencing that $Sn_2P_2S_6$ represents a direct-band semiconductor [19]. At the same time, the studies [13–17] ascertained that the high-energy part of the absorption edge for the $Sn_2P_2S_6$-type crystals obeys the Urbach rule. In this relation we would stress that the same is true for a number of perovskites [19] and the SbSJ-type crystals [20]. In all of those compounds the fundamental absorption spectrum at small α is associated with indirect interband transitions, whereas the Urbach rule governs the spectrum at larger α.

The empirical Urbach rule represents a limiting case of a more general exponential dependence of the absorption coefficient in the short-wavelength spectral region. Two modifications of that rule might be distinguished. One of them is called as a "crystalline one" and describes temperature behaviour of the absorption edge for crystals and some glasses. The other, "glass-like one", is peculiar for the most of semiconducting glasses. The Urbach's "tail" is directly related to structural disordering of atomic lattice, either dynamical (thermal phonons) or static one ("frozen" phonons). In the case of thermal

disordering, when a dynamical temperature-induced disordering is present in the system, a temperature increase would induce changes in the slope of spectral characteristics. Then, according to the Urbach rule, the dependence of α on the phonon energy $h\nu$ and the temperature T may be described by the relation

$$\alpha(h\nu, T) = \alpha_o \exp\frac{\sigma}{kT}(h\nu - E_0), \qquad (1)$$

where

$$\sigma(T) = \sigma_0 \frac{2kT}{h\nu_0} \tanh\left(\frac{h\nu_0}{2kT}\right). \qquad (2)$$

The parameter σ is ascribed to temperature-dependent slope of the spectral dependence of absorption coefficient, σ_0 is the strength of interaction between electrons (or excitons) and phonons and $h\nu_0$ the effective phonon energy. The parameters α_o and E_0 may be found as coordinates of the focal point, at which the spectral dependences of the absorption coefficient for different temperatures are crossed. The width of the Urbach "tail" is defined by the characteristic energy $W = kT/\sigma$ and represents a measure of disordering. Eqs. (1) and (2) have been derived theoretically for the case of strong electron-phonon (or exciton-phonon) interactions [20], as well as within the models of thermal fluctuations or phonon field [21]. For the system where thermal disordering dominates, the Urbach rule is valid for the overall temperature range.

In what the systems with dominating static structural disordering are concerned, the Urbach rule is supplemented by a characteristic temperature-dependent slope of the spectral dependence of absorption coefficient [22]. The latter feature holds true at the temperatures higher than some point where the temperature dependence of the absorption edge becomes linear. Below this temperature point the absorption edge depends nonlinearly upon T. Following the work [23], one can find the characteristic energy W for the solid solutions as

$$W = W_T + W_x = D_D\left[\left\langle U^2 \right\rangle_T + \left\langle U^2 \right\rangle_x\right], \qquad (3)$$

where W_T denotes the temperature disordering, W_x the structural (topological) disordering, D_D the distortion potential of the characteristic energy, $\left\langle U^2 \right\rangle_T$ the mean-square deviation of atomic positions from the ideal positions in the crystalline lattice, which is caused by the temperature disordering. Finally, the parameter $\left\langle U^2 \right\rangle_x$ means the structural disordering.

Phenomenological analysis of the exponential absorption edge described by Eq. (1) and its behaviour in the course of phase transitions has been performed in the work [24]. It is evident that any changes in the electron-phonon (exciton-phonon) interaction occurred at a phase transition can impose corresponding changes in the parameters entering the Urbach rule. In its turn, the exact character of those changes defines the main

peculiarities of the absorption edge observed at the phase transition.

Depending on which of the three parameters change at the phase transition, we can observe experimentally one or two convergence points of the $\ln\alpha(h\nu)$ curves measured at different temperatures. If, for example, E_0 and α_0 are invariable in the vicinity of the phase transition and σ quantity alone suffers an anomaly at this transition, one should detect a single convergence point for the $\ln\alpha(h\nu)$ dependences. On the contrary, if α_0 and $\sigma(T)$ do not reveal anomalies near the point of the first-order phase transition and E_0 value changes, than there exist two separate convergence points for the $\ln\alpha(h\nu)$ dependences, which are peculiar for the paraelectric and ferroelectric phases. In the case of second-order phase transitions, one of those points can be absent, owing to continuous changes in the order parameter. At last, if E_0 and $\sigma(T)$ manifest no anomalies near the phase transition point, though the α_0 parameter changes, one observes experimentally two Urbach "fans", for which the convergence points of the $\ln\alpha(h\nu)$ dependences are shifted with respect to each other by some distance along the $\ln\alpha$ axis. In all the cases considered above, it is the parameter which changes at the phase transition that takes responsibility for the corresponding absorption edge anomalies.

Let the parameters E_o, σ and α_0 change simultaneously. Then the Urbach rule takes the following form:

$$\alpha = \alpha_0' \exp\frac{\sigma'(T)}{kT}\left[h\nu - E_0'\right]. \tag{4}$$

For this case the temperature dependence of the absorption edge may be written as

$$E_g^\alpha(T) = E_0' - \frac{kT}{\sigma'(T)}\ln\frac{\alpha_0'}{\alpha}, \tag{5}$$

where

$$E_0' = E_o + \beta\eta^2, \quad \ln\alpha_0' = \ln\alpha_o - \frac{\sigma(T_c)}{kT_c}\gamma\eta^2, \quad \sigma'(T) = \frac{\sigma(T)}{1-\left(\dfrac{\sigma(T)}{kT}\delta\eta^2\right)}. \tag{6}$$

Here the parameters β, γ and δ in Eqs. (6) are constants, the unprimed quantities E_0, α_0 and σ correspond to the paraelectric phase and э means the order parameter.

If the contributions from each anomaly are taken into account properly, the jump of the absorption edge in the region of phase transition can be determined using the relationship

$$\Delta E_g^\alpha = \beta\eta^2 + \gamma\eta^2 + \ln\left(\frac{\alpha_0}{\alpha}\right)\delta\eta^2 - \frac{\sigma(T_c)}{kT_c}\gamma\delta\eta^4. \tag{7}$$

Here the first three terms are contributions from the E_0, α_0 and σ anomalies and

the forth term represents a second-order correction. The shift of E_0 is obviously associated with the bandgap changes. The anomaly $\sigma(T)$ can be evoked, with equal probabilities, by changing strength of the electron-phonon (exciton-phonon) interaction, via the σ_0 parameter, or by a possible change of phonon coupled with electron (or exciton) in the vicinity of phase transition.

3. „Urbach" character of the absorption edge in $(Pb_ySn_{1-y})P_2(Se_xS_{1-x})_6$ crystals under atmospheric pressure

The spectral dependences $\ln\alpha(h\nu)$ shown below have been obtained on the basis of experimental measurements of the optical transmittance t and the reflectivity r of the crystals under study for the case of unpolarized light. The α parameter has been derived using the known formula

$$\alpha = \frac{1}{d}\ln\frac{(1-r)^2 + \sqrt{(1-r)^4 + 4t^2r^2}}{2t} \ , \tag{8}$$

where d is the sample thickness. The spectral resolution of our setup built on the basis of monochromator MDR-2 has been approximately $1\times10^{-3}\,\mathrm{eV}$.

Fig. 2 and 3 demonstrate $\ln\alpha(h\nu)$ dependences for the $Sn_2P_2S_6$ and $Sn_2P_2Se_6$
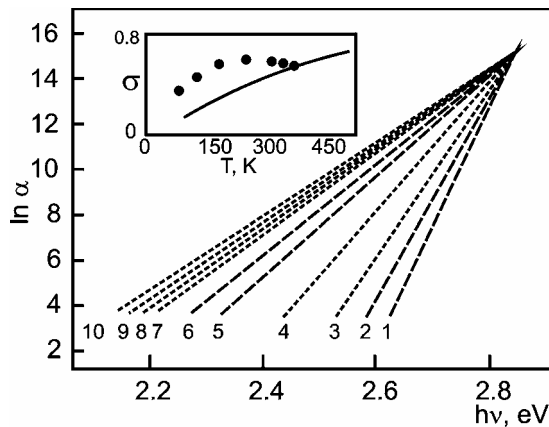
Fig. 2. Spectral dependences of $\ln\alpha$ for $Sn_2P_2S_6$ crystals at the atmospheric pressure and different temperatures: 1 – 77, 2 – 120, 3 – 180, 4 – 240, 5 – 303, 6 – 325, 7 – 345, 8 – 373, 9 – 423 and 10 – 473 K. The insert shows temperature dependence of the parameter σ [17].
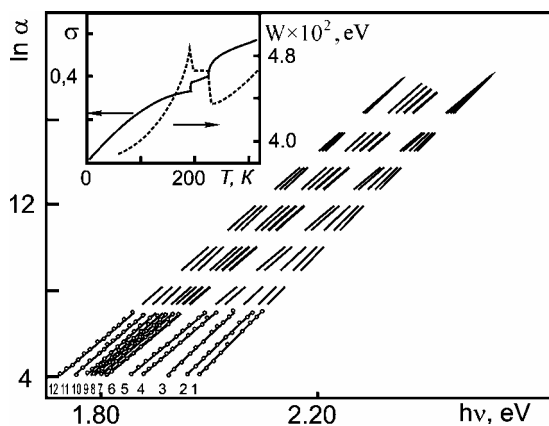
Fig. 3. Spectral dependences of $\ln\alpha$ for $Sn_2P_2Se_6$ crystals at the atmospheric pressure and different temperatures: 1 – 77, 2 – 110, 3 – 150, 4 – 180, 5 – 190, 6 – 195, 7 – 205, 8 – 210, 9 – 220, 10 – 230, 11 – 270 and 12 – 310 K.
The insert shows temperature dependences of the parameters σ and W [10].

crystals obtained at the atmospheric pressure and different temperatures. It is seen that the absorption edge shifts towards lower energies with increasing temperature. The Urbach rule holds true in both the paraelectric and ferroelectric phases. From Fig. 2 it follows that the coordinate of the convergence point of $\ln \alpha (h\nu)$ dependences for $Sn_2P_2S_6$ crystals is common for the paraelectric and ferroelectric phases. One can see from Fig. 3 that the corresponding points for the case of $Sn_2P_2Se_6$ differ for different phases. In the incommensurate phase the dependences $\ln \alpha (h\nu)$ do not converge at all, while the characteristic energy W remains constant. Note that, maybe, a first observation of violation of the Urbach rule for the incommensurate phases has been reported in the work [25] for the specific case of $[N(CH_3)_4]_2CuCl_4$ crystals. The effect has been explained in Ref. 14 on the basis of phenomenological approach. Indeed, if one-dimensional modulation of ferroelectric structure is available, one should introduce into the $E^g (P_s)$ expansion the gradient terms of the type of $(\partial P_s / \partial z)^2$ (with z being the modulation axis). Then one gets the following relations for E_0', $\ln \alpha_0'$ and σ' parameters included in Eq. (4):

$$E_0' = E_o + \beta P_s^2 + \beta' \left[\frac{\partial P_s}{\partial z} \right]^2 , \qquad (9)$$

$$\ln \alpha_0' = \ln \alpha_o - \frac{\sigma(T)}{kT} \left[\gamma P_s^2 + \gamma' \left(\frac{\partial P_s}{\partial z} \right)^2 \right] , \qquad (10)$$

$$\sigma' = \frac{\sigma(T)}{\left\{ 1 - \frac{\sigma(T)}{kT} \left[\delta P_s^2 + \delta' \left(\frac{\partial P_s}{\partial z} \right)^2 \right] \right\}} , \qquad (11)$$

where β, β', γ, γ', δ and δ' are constants. The α_0, E_0 and σ values correspond to the paraelectric phase ($P_s = 0$). The $\partial P_s / \partial z$ value changes with temperature inside the incommensurate phase [26]. For instance, for the $Sn_2P_2Se_6$ crystals this fact is directly confirmed by the X-ray structural studies [26]. As a consequence, we can consider the parameters α_0' and E_0' as dependent on temperature inside the incommensurate phase. This causes violation of the Urbach rule written in the form of Eq. (1) and results in absence of any convergence point for the $\ln \alpha (h\nu)$ dependences taken at different temperatures. Here we deal with a temperature-independent slope of spectral curves of the absorption coefficient. The latter result points to a deciding role of static structural disordering in the effect. Our conclusion agrees well with an idea that the incommensurate phase represents a crystalline state similar to that of the dipole glass [6].

When the temperature decreases in the region of incommensurate phase near the

$T = T_c$ point, a first-order phase transition into ferroelectric state happens, accompanied by a jump-like disappearance of the structural modulation ($(dP_s/dz)^2 = 0$). Deep inside the ferroelectric phase, i.e. away from T_c, the P_s value hardly depends upon temperature. Then the parameters α_0 and E_0 virtually do not changes and we observe the same Urbach "fan".

The parameters α_0 and E_0 for $Sn_2P_2S_6$ and $Sn_2P_2Se_6$ crystals and the solid solutions on their basis are gathered in Table 1. It is clearly seen that the substitution $S \rightarrow Se$ decreases the E_0 value, though the parameter α_0 then increases. The experimental values σ_0 obtained for the solid solutions $Sn_2P_2(Se_{1-x}S_x)_6$ of different

Table 1. Some parameters of ferroelectrics-semiconductors of $A_2^{IV}B_2^{V}C_6^{VI}$ group in the ferroelectric (FP) and paraelectric (PP) phases [10].

Crystals	$x(y)$, mol.%	Parameters											
		E_0, eV		$\ln \alpha_0$		ν_0, cm^{-1}		$\sigma_0, 10^{-1}$		$-\dfrac{dE_g^\alpha}{dT}$, 10^{-3}eV/K		$-\dfrac{dE_g^\alpha}{dp}$, 10^{-2}eV/GPa	
		PP	FP	PP	FP	PP	FP	PP	FP	PP	FP	PP	FP
$Sn_2P_2(Se_{1-x}S_x)_6$	0	2.86	2.86	15.95	15.95	142	–	9.7	6.8	0.58	2.67	8	57.6
	0.1	–	–	–	–	–	–	–	–	0.62	2.86	8	62.1
	0.2	–	–	–	–	–	–	–	–	0.63	3.06	7.6	68
	0.3	2.50	2.63	16.80	16.74	145	169	6.20	5.84	0.71	1.36	8.2	–
	0.6	–	–	–	–	–	–	–	–	–	–	8.4	–
	1.0	2.36	2.53	17.75	17.99	89	104	5.30	4.98	0.56	0.83	8.3	–
$(Pb_ySn_{1-y})_2P_2S_6$	0.05	2.60	2.96	10.90	9.75	263	206	5.10	4.60	0.70	2.27	7.5	41.5
	0.1	2.55	2.79	9.70	12.10	257	198	4.15	3.35	0.68	1.54	7.8	–
	0.2	2.64	2.78	11.50	13.10	242	152	5.21	3.92	0.66	1.44	6.2	–
	0.3	2.58	2.72	10.80	13.50	249	156	4.70	4.70	0.57	1.37	5.0	–
	0.4	2.61	2.61	10.80	10.80	248	156	4.85	3.84	0.51	1.00	4.0	–
	0.6	2.77	–	12.46	–	254	–	4.60	–	0.64	–	3.5	–
	0.8	2.86	–	11.95	–	250	–	3.85	–	0.81	–	2.4	–
$(Pb_ySn_{1-y})_2P_2Se_6$	0.05	1.94	2.09	9.12	9.83	260	236	5.69	3.64	0.38	1.25	8.2	–
	0.2	1.99	2.06	10.75	9.95	350	109	7.05	2.57	0.29	0.71	7.2	–
	0.35	2.22	–	13.99	–	274	–	5.58	–	0.51	–	5.8	–
	0.8	2.25	–	14.15	–	370	–	7.78	–	0.56	–	3.6	–
	1.0	2.34	–	15.89	–	274	–	8.90	–	0.71	–	3.3	–

contents prove a strong electron-phonon interaction in these crystals ($\sigma_0 < 1$). A transition from the paraelectric phase into ferroelectric one gives rise to decreasing σ_0, thus indicating a strengthened electron-phonon interaction. As seen from Table 1, strengthening of the interaction also can originate from increasing Se content in the solid solutions $Sn_2P_2(Se_{1-x}S_x)_6$, evidently, due to decreased ionicity of the corresponding bonds. The experimental values v_0 obtained for the above solid solutions correlate well with the true frequencies of fully symmetric deformation vibrations of $[P_2S(Se)_6]^{4-}$ ions. The latter frequencies have been derived from the Raman spectra of $Sn_2P_2S_6$ crystals and compared to those found in the spectra of their chemical analogs, including $[P_2S(Se)_6]^{4-}$ ion [27]. Apparently, this compasses us to the conclusion that the exponential dependence of the absorption edge peculiar for the crystals under study is stipulated by interaction of electrons with the phonons responsible for the vibrations of anionic complexes $[P_2S(Se)_6]^{4-}$. The frequency of those phonons is sensitive to the isomorphous substitution of S for heavier Se atom, though does not depend on the ionic substitution $Sn \rightarrow Pb$.

Fig. 4 displays the temperature dependences of $\ln\alpha$ for the crystals of $Sn_2P_2(Se_{0.30}S_{0.70})_6$ at different temperature. It is seen that, similarly to the solid solutions of $Sn_2P_2Se_6$, the Urbach rule is fulfilled for the absorption edge, with the dependences $\ln\alpha(hv)$ converging at the points that differ for different phases. In the case of ferroelectric phase we have $T < T_c = 280\,\mathrm{K}$, $\alpha_0' = (10.85 \pm 1.19) \times 10^6\ \mathrm{cm^{-1}}$ and $E_0' = 2.625 \pm 0.008\ \mathrm{eV}$, while for the paraelectric phase $T > T_c = 280\ \mathrm{K}$, $\alpha_0 = (2.68 \pm 0.51) \times 10^6\ \mathrm{cm^{-1}}$ and $E_0 = 2.495 \pm 0.010\ \mathrm{eV}$.
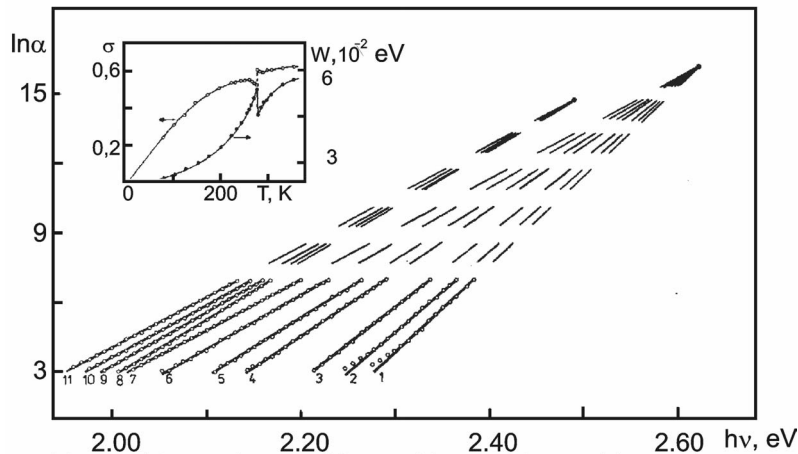
Fig. 4. Dependences of $\ln\alpha(hv)$ for $Sn_2P_2(Se_{0.30}S_{0.70})_6$ crystals at different temperatures: 1 − 77, 2 − 123, 3 − 173, 4 − 223, 5 − 244, 6 − 268, 7 − 278, 8 − 281, 9 − 300, 10 − 310 and 11 − 333 K. The insert shows temperature dependences of the parameters σ and W [13].

The temperature dependences of σ and W parameters are also presented in Fig. 4. One can see a clearly visible jump at $T = T_c$. On the whole, the temperature behaviour of σ obeys Eq. (2). Then one obtains $\sigma_0' = 0.584$ and $h\nu_0 = 0.0210$ eV for the ferroelectric phase and $\sigma_0 = 0.620$ and $h\nu_0 = 0.0180$ eV for the paraelectric one. Hence, the jump observed in the $\sigma(T)$ dependence at $T = T_c$ is caused by changes in both the electron-phonon interaction strength ($\Delta\sigma_0 = 0.036$) and the effective phonon energy ($\Delta h\nu_0 = 0.0030$ eV). It is worth emphasizing that the jump $\Delta\sigma(T)$ is accompanied by a preliminary extremum observed in the $\sigma(T)$ dependence not far from the phase transition point. Obviously, the effect should be linked with fluctuations of P_s near the Lifshitz point. Thus, all the three parameters governing the Urbach rule change in the course of phase transition occurring in $Sn_2P_2(Se_{0.30}S_{0.70})_6$ crystal. Along with the jump of the absorption edge, this enables us to identify the phase transition with a first-order one. After comparing the experimental results with Eqs. (6), the authors [13] have calculated the quantities $\beta\eta^2$, $\gamma\eta^2$ and $\delta\eta^2$, which turn out to be equal to 0.13, -5.6×10^{-2} and -5.5×10^{-3} eV, respectively. According to Eq. (7), the jump ΔE_g^α at the phase transition in $Sn_2P_2(Se_{0.30}S_{0.70})_6$ found for the fixed value $\alpha = 150$ cm^{-1} equals to 0.012 eV.
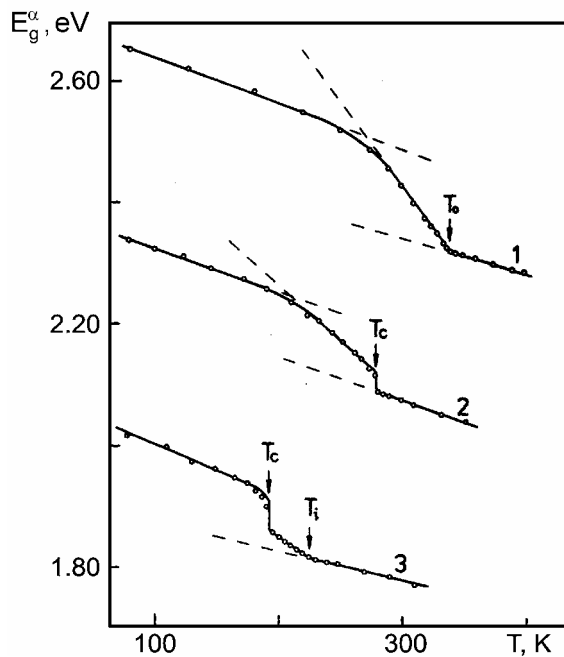
Fig. 5. Temperature dependences of $E_g^\alpha\left(\alpha = 150 \text{ cm}^{-1}\right)$ for $Sn_2P_2S_6$ (1), $Sn_2P_2(Se_{0.30}S_{0.70})_6$ (2) and $Sn_2P_2Se_6$ (3) crystals at $p=p_{atm}$.

In Fig. 5 we plot the temperature dependences of E_g^α (at $\alpha = 150$ cm^{-1}) for the three crystals from the $Sn_2P_2(Se_xS_{1-x})_6$ series obtained at the atmospheric pressure. It is evident that the $E_g^\alpha(T)$ dependence for the $Sn_2P_2S_6$ crystal shows a break in the vicinity of $T = T_0 = 339$ K, which is imposed by the second-order ferroelectric phase transition. The temperature coefficients characterizing the shift of the absorption edge in the ferroelectric and paraelectric phases are 26.57×10^{-4} and 5.83×10^{-4} eV/K, respectively. There exists another anomaly in

$E_g^\alpha(T)$ observed inside the ferroelectric phase close to $T = 280$ K. It is induced by pinning of domain walls by defects of crystal lattice.

Hence, the dependences $E_g^\alpha(T)$ for $Sn_2P_2S_6$ show three regions where the absorption edge shifts linearly with temperature. It is seen from curve 2 that the $E_g^\alpha(T)$ dependence for the $Sn_2P_2(Se_{0.30}S_{0.70})_6$ crystal is very similar to those considered above, except for the jump $\Delta E_g^\alpha = (0.030 \pm 0.005)$ eV at $T = 280$ K related to the first-order phase transition. The anomaly E_g^α in the ferroelectric phase associated with pinning of the domain walls at the defects is located close to $T = 220$ K. Curve 3 corresponds to the $Sn_2P_2Se_6$ crystal. The absorption edge jumps at $T = T_c = 193$ K ($\Delta E_g^\alpha = (0.052 \pm 0.003)$ eV) and the coefficient dE_g^α/dT changes its value at $T = T_i = 221$ K. Finally, in the incommensurate phase the dependence $E_g^\alpha(T)$ has a linear character in the temperature region of $\Delta T = 193 - 221$ K.

The experimental results shown in Fig. 5 agree with the data obtained for the phase x,T-diagram of $Sn_2P_2(Se_xS_{1-x})_6$. Let us remind that this diagram predicts a change in the order of phase transitions occurred at $x = 0.28$ and $p = p_{atm}$, splitting of the line of ferroelectric phase transitions and the appearance of incommensurate phase, which is caused by availability of the Lifshitz point. In Table 1 we present the coefficients $\left(\partial E_g^\alpha/\partial T\right)_p$ typical for the solid solutions under test. One can see that the above coefficients for the ferroelectric phase are essentially larger than those for the paraelectric phase, perhaps, owing to existence of P_s.

The solid solutions $(Pb_ySn_{1-y})_2P_2S_6$ form a continuous series, while the isomorphous ionic substitution $Sn \to Pb$ at $p = p_{atm}$ leads to lowering phase transition temperature, without changing the order of the phase transition. The spectral dependences of $\ln\alpha$ for the $(Pb_{0.4}Sn_{0.6})_2P_2S_6$ crystals at different temperatures are depicted in Fig. 6. One can see that the absorption edge obeys the Urbach rule in the overall range of α and $h\nu$, revealing a single convergence point for the both structural phases. Increasing temperature shifts the absorption edge towards the region of lower energies. The experimental values of E_0 and α_0 almost do not vary and are equal to $E_0 = 2.61$ eV and $\ln\alpha_0 = 10.80$. Transition to the ferroelectric phase is accompanied by decreasing σ_0 and ν_0 parameters. The given crystals manifest a strong electron-phonon interaction, too. Within the accuracy limits ($\Delta\nu_0 = \pm 12\,cm^{-1}$), the isomorphous ionic substitution hardly affects the H_0 value observed for the solid solutions. The H_0 values presented in Table 1 agree well with the data reported in the Raman spectra study [28].
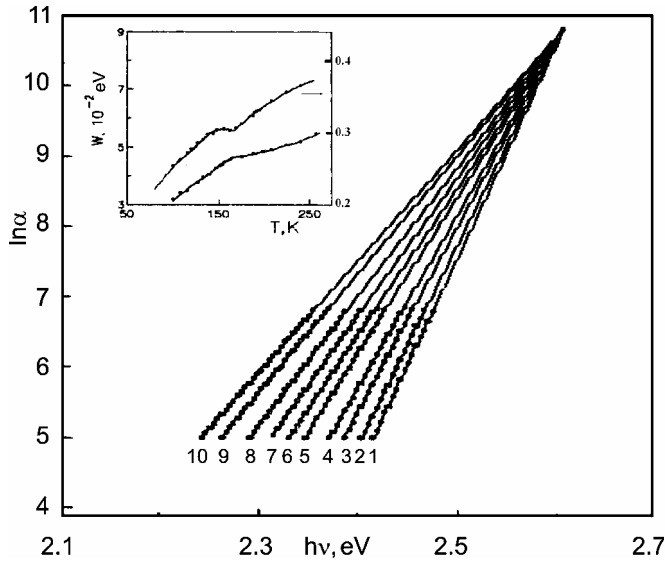
Fig. 6. Dependences of $\ln\alpha(h\nu)$ for $(Pb_{0.4}Sn_{0.6})_2P_2S_6$ and $(Pb_{0.4}Sn_{0.6})_2P_2S_6$ crystals at $p = p_{atm}$ and different temperatures: 1 – 100, 2 – 109, 3 – 126, 4 – 137, 5 – 159.5, 6 – 188, 7 – 223, 8 – 256.5, 9 – 299 and 10 – 318 K.

The insert shows temperature dependences of σ and w parameters [10].

The vibration frequencies 249 and $260\,cm^{-1}$ found for $[P_2S_6]^{-4}$ ion correspond to degenerated deformation vibrations of P-S-P bond of E_y type. The temperature and the isomorphous ionic substitution do not essentially affect those vibrations. Using Eqs. (4)–(6), the authors [15] have calculated the values of $\beta\eta^2$, $\gamma\eta^2$ and $\delta\eta^2$ at $\alpha = 400\,cm^{-1}$. For instance, for the case of solid solution $(Pb_{0.2}Sn_{0.8})_2P_2S_6$ they are equal respectively to 14.0, -8.2 and $-1.0\times10^{-2}\,eV$. Fig. 6 testifies that the temperature dependences of σ and W reveal the anomalies in the region of phase transition, which are typical for second-order phase transitions.

In Fig. 7 we show the spectral dependences of the absorption coefficient for $(Pb_{0.05}Sn_{0.95})_2P_2Se_6$ in the wide temperature region and at $p = p_{atm}$ [14]. Here the incommensurate phase exists in the region $\Delta T = 33K$. The absorption edge in the ferroelectric and paraelectric phases has exponential character and obeys the Urbach rule, though the dependences $\ln\alpha(h\nu)$ reveal different convergence points under temperature changes. There is no convergence point for the $\ln\alpha(h\nu)$ dependences in the incommensurate phase. When the temperature increases, the absorption edge is shifted towards the low-energy region. As seen from Fig. 7, the temperature dependences of the absorption edge position include peculiarities near the phase transition points, although those dependences remain linear in the regions of paraelectric, incommensurate and ferroelectric phases. The dependence $E_g^{\alpha}(T)$ suffers a break-like anomaly in the vicinity of the phase transition at T_i, which testifies the second-order structural transformation.

In the region of phase transition at T_c the $E_g^{\alpha}(T)$ dependence shows jump characteristic of first-order phase transitions. As seen from Table 1, the coefficients
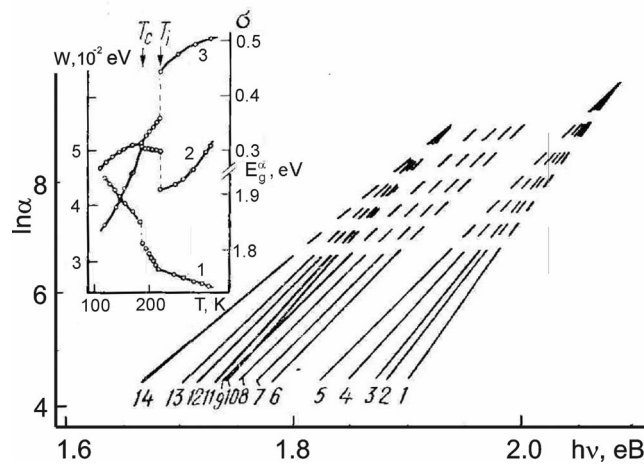
Fig. 7. Spectral dependences of $\ln \alpha$ for $(Pb_{0.05}Sn_{0.95})_2P_2Se_6$ crystals at $p = p_{atm}$ and different temperatures: 1 – 112, 2 – 135, 3 – 146, 4 – 164, 5 – 180, 6 – 187, 7 – 196, 8 – 204, 9 – 212, 10 – 240, 11 – 253, 12 – 261, 13 – 303 and 14 – 324 K. The insert shows temperature dependences of E_g^α at $\alpha = 150\,cm^{-1}$ (1), W (2) and y (3) [14].

dE_g/dT for those solid solutions taken in the ferroelectric phase are notably larger than those for the paraelectric phase, evidently due to existence of spontaneous polarization in the former phase. Like the other solid solutions of the mentioned group, the $\sigma(T)$ dependence for the $(Pb_ySn_{1-y})_2P_2Se_6$ crystals is well described by Eq. (2), with the σ_0 and ν_0 parameters different for the paraelectric and ferroelectric phases. At T_c we observe the changes in both the electron-phonon interaction strength and the energy of phonons participating in formation of the absorption edge. Inside the incommensurate phase the parameter σ increases linearly with temperature, though the slope of the absorption edge is invariable. The parameters σ and W suffer jumps at the temperature of phase transition from incommensurate to paraelectric phase.

Hence, the temperature studies of the absorption edge in ferroelectrics-semiconductors of $A_2^{IV}B_2^{V}C_6^{VI}$ group at the atmospheric pressure have shown that the $\ln \alpha(h\nu)$ dependences in their high-energy parts obey the Urbach rule and the electron-phonon interaction is strong enough. Exponential shape of the absorption edge is associated with interaction of electron subsystem with phonons corresponding to deformation vibrations of the anionic complexes $\left[P_2S(Se)_6\right]^{-4}$. The Urbach rule is violated inside the incommensurate phase, which is caused by dependence of its parameters upon the temperature. Isomorphous substitution $Sn \rightarrow Pb$ in the cationic sublattice of $Sn_2P_2S_6$ increases the bandgap and the $S \rightarrow Se$ substitution decreases the E_g value.

4. Influence of hydrostatic pressure on the absorption edge in $(Pb_ySn_{1-y})_2P_2(Se_xS_{1-x})_6$ crystals. Role of electron-phonon interaction in the temperature bandgap changes

Taking temperature and baric dependences of the absorption edge into account, we modify Eq. (5) as follows:

$$E_g^\alpha(T,p) = E_0(p) - \frac{kT}{\sigma(T,p)}\ln\frac{\alpha_0(p)}{\alpha} = E_0(p) - W(T,p)\ln\frac{\alpha_0(p)}{\alpha}. \qquad (12)$$

The dependence $E_g^\alpha(T)$ at a constant pressure is defined by the term $W(T)$. However, the dependence E_g^α on pressure at a constant temperature can be defined by changes in both the W parameter and the E_0 and α_0 parameters. The baric changes of W, E_0 and α_0 inside the same phase may be represented in the simplest linear approximation as

$$\alpha_0(p) = \alpha_0(0) + \alpha_0 p, \quad E_0(p) = E_0(0) + b_0 p, \quad W(T,p) = W(T,0) + c_0 p. \qquad (13)$$

As seen from Fig. 8 and 9, $Sn_2P_2S_6$ and $Sn_2P_2Se_6$ crystals demonstrate a parallel baric shift of the absorption edge, thus pointing out that the characteristic energy W is kept invariable. Within the paraelectric phase the α_0 value does not depend on external pressure [29], so that the baric behaviour of E_g^α in those crystals is determined by the $E_0(p)$ dependence alone. The latter is confirmed by equality of the coefficients dE_g^α/dp and dE_0/dp.

Unlike with the $Sn_2P_2S_6$ and $Sn_2P_2Se_6$ compounds, the W parameter for the solid solutions $Sn_2P_2(Se_xS_{1-x})_6$ (x = 0.3, 0.6 and 0.8) decreases with increasing pressure. In particular, this is proved by the experimental results shown in Fig. 10. Decrease in the W value under overall compression evidences a structural ordering of $Sn_2P_2(Se_{0.3}S_{0.7})_6$
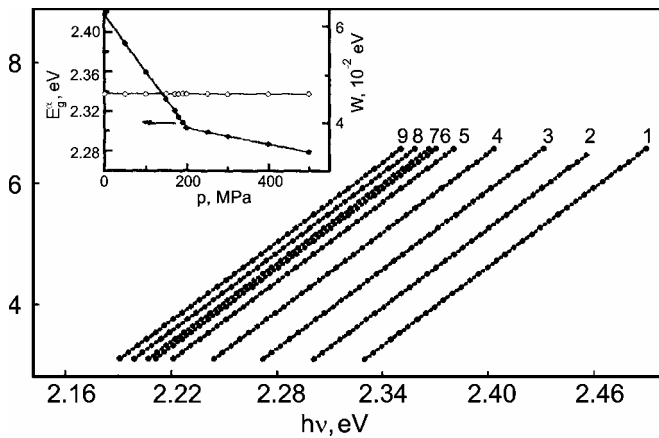
Fig. 8. Dependences of $\ln\alpha(h\nu)$ for $Sn_2P_2S_6$ crystals at $T = 296$ K and different pressures p: $1-5$, $2-50$, $3-100$, $4-150$, $5-190$, $6-250$, $7-300$, $8-400$ and $9-500$ MPa. The insert shows dependences $E_g^\alpha(p)$ and $W(p)$ [29].
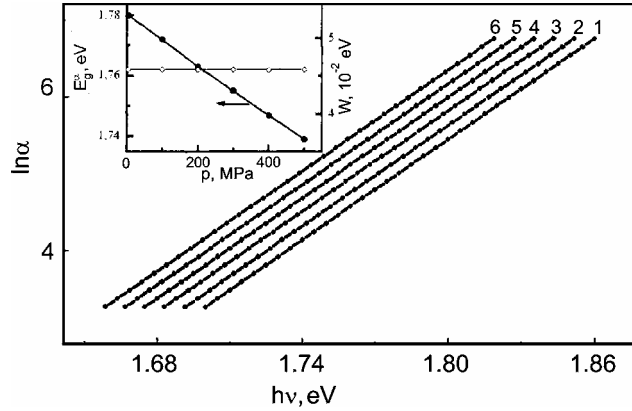
Fig. 9. Dependences of $\ln\alpha(h\nu)$ for $Sn_2P_2Se_6$ crystals at $T = 296\,K$ and different pressures p: $1 - 5$, $2 - 100$, $3 - 200$, $4 - 300$, $5 - 400$ and $6 - 500$ MPa. The insert shows dependences $E_g^\alpha(p)$ and $W(p)$ [29].
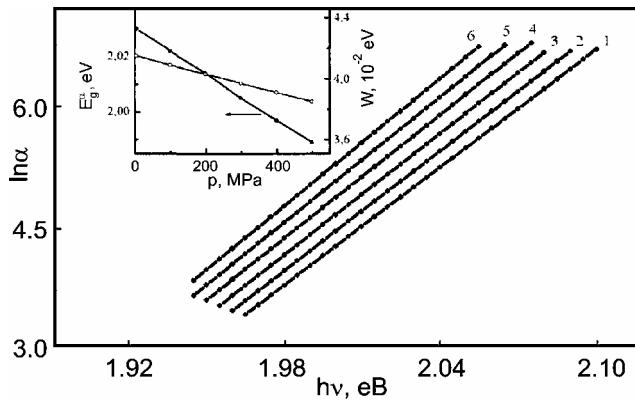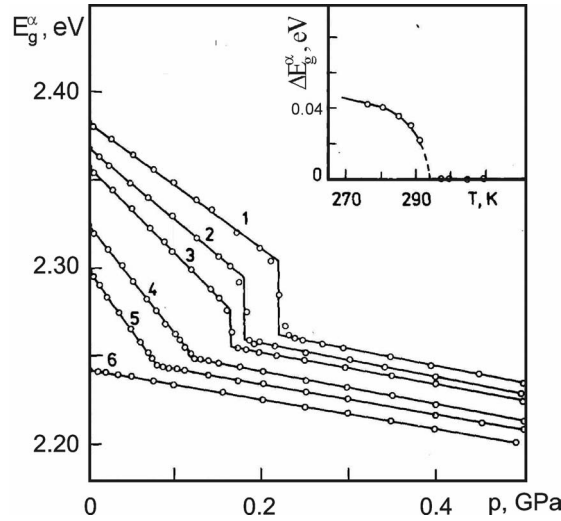

Fig. 10. Dependences of $\ln\alpha(h\nu)$ for $Sn_2P_2(Se_{0.3}S_{0.7})_6$ crystals at $T = 296\,K$ and different pressures p: $1 - 5$, $2 - 100$, $3 - 200$, $4 - 300$, $5 - 400$ and $6 - 500$ MPa. The insert shows dependences $E_g^\alpha(p)$ and $W(p)$ [29].

crystal. For the case of $Sn_2P_2(Se_{0.3}S_{0.7})_6$, $Sn_2P_2(Se_{0.6}S_{0.4})_6$ and $Sn_2P_2(Se_{0.8}S_{0.2})_6$ solid solutions, the values of $c_0 = dW/dp$ are -6.06×10^{-3}, 10.23×10^{-3} and $-8.69\times10^{-3}\,eV/GPa$, respectively. The coefficients b_0 characterizing pressure-induced changes in the E_0 parameter for the crystals mentioned are equal to -0.388, -0.532 and $-0.440\,eV/GPa$, respectively.

In this respect $Sn_2P_2(Se_{0.3}S_{0.7})_6$ crystals represent a specific case. It is characterized by a decrease in α_0 under the influence of pressure, besides of decreasing W and E_0 parameters. At the atmospheric pressure the coordinates of the convergence point for the temperature dependences of $\ln\alpha(h\nu)$ found for the above crystals are $\alpha_0 = 2.680\times10^6\,cm^{-1}$ and $E_0 = 2.495\,eV$, while at the pressure $p = 500\,MPa$ they become $\alpha_0 = 0.361\times10^6\,cm^{-1}$ and $E_0 = 2.301\,eV$. Hence, application of hydrostatic pressure to the $Sn_2P_2(Se_{0.3}S_{0.7})_6$ crystals leads to decrease in all the three parameters entering the Urbach relation, similarly to the other solid solutions of the series. Hydrostatic compression of the solid solutions $(Pb_ySn_{1-y})_2P_2(Se_xS_{1-x})_6$ and $Sn_2P_2(Se_xS_{1-x})_6$ imposes a parallel shift of the absorption edge to lower energies. Then the baric dependence of E_g^α parameter results from the corresponding variations of α_0, σ_0 and E_0.

Let us now consider behaviour of the absorption edge near the Lifshitz point on the example of $Sn_2P_2(Se_{0.04}Sn_{0.96})_6$ crystals. The baric dependences of E_g^α at different T are plotted in Fig. 11. Curve 6 is obtained at the temperature $T = 334\,K$, i.e. inside the paraelectric phase. It is seen that E_g^α decreases linearly with increasing pressure. The

Fig. 11. Baric dependences of $h\nu_\alpha$ $\left(\alpha = 150\,cm^{-1}\right)$ for $Sn_2P_2(Se_{0.04}S_{0.96})_6$ crystal at different temperatures T: 1 – 276, 2 – 285, 3 – 290, 4 – 300, 5 – 309.5 and 6 – 334 K. The insert shows temperature dependence of the jumps $\Delta h\nu_\alpha$ [30].

dependence $E_g^\alpha(p)$ has different character for the case of ferroelectric phase. At the temperatures $T = 309.5$ and $T = 300\,K$, the baric dependences of E_g^α manifest breaks respectively at $p = 0.08$ and $0.125\,GPa$, which represent characteristic features of the second-order phase transitions. The phase transition in those crystals has a continuous character right up to the Lifshitz point, the coordinates of which on the p,T-diagram of $Sn_2P_2(Se_{0.04}Sn_{0.96})_6$ are $T_L = (293 \pm 2)\,K$ and $p_L = (0.014 \pm 0.050)\,GPa$. If the pressure is higher and the temperature lower than those corresponding to the Lifshitz point, the dependences $E_g^\alpha(p)$ include jumps (see curves 1 to 3), confirming availability of the first-order phase transition. In Fig. 11 we also show the of the jumps ΔE_g^α along the p,T-diagram. After extrapolation $\Delta E_g^\alpha \to 0$ one can determine the temperature for which a change in the phase transition order takes place.

Temperature dependences of energy positions of the absorption edge for the $(Pb_{0.1}Sn_{0.9})_2P_2S_6$ crystals at different pressures are shown in Fig. 12. It is seen that a character of $E_g^\alpha(T)$ dependences changes with increasing pressure. In the pressure region of $p < 0.27\,GPa$, the coefficients $\Delta\left(\dfrac{\partial E_g^\alpha}{\partial p}\right)$ reveal jumps as a result of second-order phase transition. Under the influence of pressure, the anomalies in the $E_g^\alpha(T)$
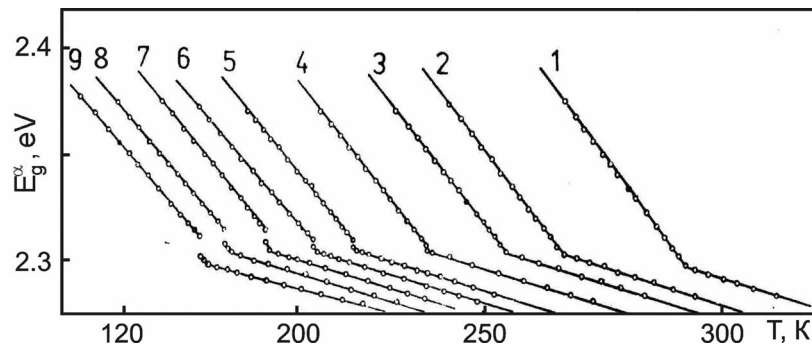
Fig. 12. Temperature dependences of E_g^{α} ($\alpha = 400\,\text{cm}^{-1}$) for $(\text{Pb}_{0.1}\text{Sn}_{0.9})_2\,\text{P}_2\text{S}_6$ crystals at different pressures p: 1 – 0001, 2 – 0.13, 3 – 0.19, 4 – 0.27, 5 – 0.35, 6 – 0.39, 7 – 0.44, 8 – 0.48 and 9 – 0.50 GPa [16].

dependences occurring at the phase transition shift towards lower temperatures. In the region of $p > 0.27\,\text{GPa}$ the phase transition is accompanied by the jumps in ΔE_g^{α}, testifying the first-order phase transition. When the p parameter increases and, correspondingly, the phase transition temperature decreases along the p,T-diagram, the jumps ΔE_g^{α} increase, signifying that a first-order character of the phase transition becomes more pronounced. It is seen from the $E_g^{\alpha}(T)$ dependences (curves 5 to 9) that some breaks occur at T_i, besides of the ΔE_g^{α} jumps at T_c.

The baric coefficient may be determined from the relation

$$-\frac{dT_c}{dp} = \Delta\left(\frac{\partial E_g}{\partial p}\right)_T \bigg/ \Delta\left(\frac{\partial E_g}{\partial T}\right)_p . \tag{14}$$

Inserting the jumps $\Delta\left(\dfrac{\partial E_g^{\alpha}}{\partial p}\right)_T$ and $\Delta\left(\dfrac{\partial E_g^{\alpha}}{\partial T}\right)_p$ into Eq. (14) [20], one can find the pressure coefficients for the Curie temperature for the case of solid solutions $(\text{Pb}_y\text{Sn}_{1-y})_2\text{P}_2\text{S}_6$ and $\text{Sn}_2\text{P}_2(\text{Se}_x\text{S}_{1-x})_6$. It is evident from Table 2 that dT_0/dp values calculated on the basis of purely optical studies correlate well with the results of other measurements (see Table 2), thus testifying validity of Eq. (14).

Table 1 summarizes the results for the baric coefficients dE_g^{α}/dp derived for different $\text{Sn}_2\text{P}_2\text{S}_6$-based solid solutions. Obviously, increasing y content in the solid solutions of $(\text{Pb}_y\text{Sn}_{1-y})_2\text{P}_2(\text{Se}_x\text{S}_{1-x})_6$ induces decrease in the dE_g^{α}/dp value. This result is quite expected, since the substitution of Sn for Pb increases "overlapping" of cations with anions, and the cation-anion bonds become less compliant for compression [6]. Perhaps, this fact is the reason for pressure-induced decrease in the temperature width of incommensurate phase taking place at increasing y (see [31]). On the contrary, the

increase in x for the solid solutions $Sn_2P_2(Se_xS_{1-x})_6$ mainly leads to increasing dE_g^α/dp coefficient.

Table 2. Some characteristics of phase transitions for the solid solutions $Sn_2P_2(Se_xS_{1-x})_6$ and $(Pb_ySn_{1-y})_2P_2S_6$ [29].

$x(y)$, mol. %	$-\Delta\left(\dfrac{\partial E_g^\alpha}{\partial T}\right)_p, 10^{-3}\dfrac{eV}{K}$	$-\Delta\left(\dfrac{\partial E_g^\alpha}{\partial p}\right)_T, 10^{-2}\dfrac{eV}{GPa}$	$-\dfrac{dT_0}{dp}, \dfrac{K}{GPa}$
$Sn_2P_2(Se_xS_{1-x})_6$			
0	2.09	49.6	240
0.01	2.24	54.1	242
0.20	2.43	60.4	249
$(Pb_ySn_{1-y})_2P_2S_6$			
0.05	1.57	38.0	242
0.10	0.86	21.7	252

Let us use the experimental results of temperature and baric studies of E_g and involve additionally the data for the volume compressibility χ and the thermal expansion coefficient β. This allows estimating the role of electron-phonon interaction parameter $(dE_g/dT)_V$ in the temperature variations of the bandgap of ferroelectrics-semiconductors:

$$\left(\frac{\partial E_g}{\partial T}\right)_p = \left(\frac{\partial E_g}{\partial T}\right)_V - \frac{\beta^*}{\chi^*}\left(\frac{\partial E_g}{\partial p}\right)_T. \tag{15}$$

The results of the corresponding calculations performed for $(Pb_ySn_{1-y})_2P_2(Se_xS_{1-x})_6$ are shown in Table 3.

It is seen from Table 3 that the second term in the r. h. s. of Eq. (15) is almost two orders of magnitude less than the first one. Thus, the temperature decrease in E_g observed in the crystals under study is mainly caused by the electron-phonon interaction.

Greater $m = \left(\dfrac{\partial E_g^\alpha}{\partial T}\right)_V \left[\dfrac{\alpha_V}{\chi_V}\left(\dfrac{\partial E_g^\alpha}{\partial p}\right)_T\right]^{-1}$ coefficient for higher Pb concentrations in the $(Pb_ySn_{1-y})_2P_2S_6$ and $(Pb_ySn_{1-y})_2P_2Se_6$ crystals confirms strengthening of electron-phonon interaction in those solid solutions. The substitution $Se \rightarrow S$ in the $Sn_2P_2(Se_xS_{1-x})_6$ crystals affects neither the coefficient m nor the deformation potential

$$D_g = \frac{1}{\chi_V}\frac{dE_g^\alpha}{dp}. \tag{16}$$

Table 3. Some parameters of $(Pb_ySn_{1-y})_2P_2(Se_xS_{1-x})_6$ crystals [29].

Parameter Crystal	$y(x)$, mol.%	$\left(\dfrac{dE_g^\alpha}{dT}\right)_V \times 10^{-4}$, eV/K	$\dfrac{\alpha_V}{\chi_V}\left(\dfrac{dE_g^\alpha}{dp}\right)_T \times 10^{-4}$, eV/K	$-D_g$, eV	m
$(Pb_ySn_{1-y})_2P_2S_6$	0.05	−8.46	−1.48	2.24	5.7
	0.1	−8.33	−1.55	2.35	5.4
	0.2	−7.81	−1.26	2.15	6.2
	0.3	−6.70	−1.04	1.58	6.4
	0.4	−5.96	−0.86	1.30	7.0
	0.6	−6.96	−0.56	085	12.4
	0.8	−8.67	−0.57	0.86	15.3
$Sn_2P_2(Se_xS_{1-x})_6$	0	−7.2	−1.41	2.35	5.1
	0.1	−7.36	−1.42	2.36	5.2
	0.3	−8.5	−1.38	2.38	6.3
	0.8	−7.2	−1.33	2.44	5.4
	1	−9.6	−1.27	2.35	5.4
$(Pb_ySn_{1-y})_2P_2Se_6$	0.05	−5.2	−1.43	2.33	3.6
	0.2	−4.2	−1.40	2.21	3.0
	0.35	−6.2	−1.11	1.94	5.6
	0.8	−6.3	−0.74	1.35	8.5
	1	−7.8	−0.68	1.26	11.5

5. Indirect optical transitions in $(Zn_{0.05}Sn_{0.95})_2P_2S_6$ crystals under high pressure

$(Zn_{0.05}Sn_{0.95})_2P_2S_6$ crystals represent a ferroelectric semiconductor. Their temperature of the second-order phase transition ($T_0 = 341\,K$) is 2 K higher than that of $Sn_2P_2S_6$ [32]. Studies of their p,T-diagram have testified presence of the Lifshitz point at $p \simeq 0.1\,GPa$ and $T = 310\,K$, which divides the transitions into ferroelectric, incommensurate and paraelectric phases. It has also been revealed that the absorption edge for the ferroelectric and paraelectric phases in its high-energy part has exponential shape and obeys the Urbach rule.

At the same time, some deviations of the dependence $\ln\alpha(h\nu)$ from a straight line have been detected for a number of samples in low-energy part of the absorption edge. It has been assumed that the effect might be linked with indirect optical transitions, similarly to $Sn_2P_2S_6$. In order to verify the above assumption, comprehensive studies have been undertaken for the influence of temperature and hydrostatic pressure on the absorption edge observed in the mentioned crystals. Fig. 13 shows the experimental dependences $\alpha^{\frac{1}{2}}(h\nu)$ measured at the pressure of $p = 0.25\,GPa$ and different temperatures. It is seen that the dependences manifest breaks. According to the theory,
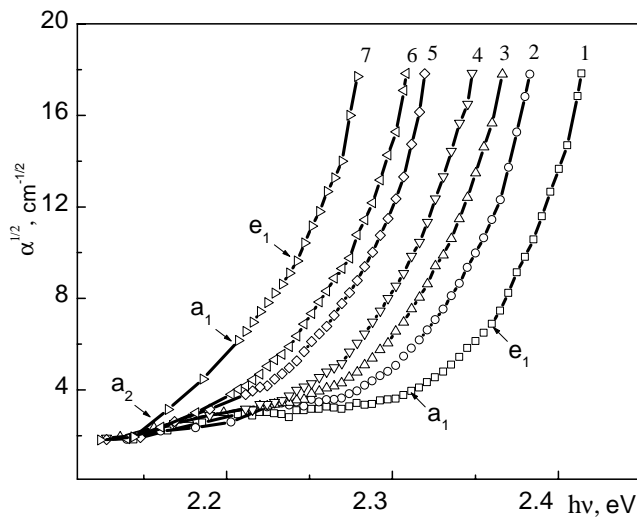
Fig. 13. Spectral dependences of $\alpha^{1/2}$ at different temperatures and $p = 0.25$ GPa for the $(Zn_{0.05}Sn_{0.95})_2P_2S_6$ crystals:
1 – 231.1 K,
2 – 245.3 K,
3 – 254.2 K,
4 – 265.4 K,
5 – 274.4 K,
6 – 278.4 K,
7 – 324.4 K.

they should be imposed by indirect optical transitions. The notations a_1 and e_1 correspond to the breaks caused respectively by absorption and emission of phonons in the main region of the absorption edge. From Fig. 13 one can see that the slopes of $\alpha^{\frac{1}{2}}(h\nu)$ dependences decrease in that region when the temperature decreases. The latter is produced by "freezing" of the phonons participating in indirect optical transitions.

In order to prevent additional errors in determining shape of the absorption edge for the case of crystals possessing phase transitions, Maclean has suggested a special technique [33] . According to that technique, one finds on the absorption edge the main region and the corresponding abscissas of the breaks ε_{a_1} and ε_{e_1} resulted from the absorption and emission of phonon. Then the indirect bandgap E_g^i and the energy of phonons $k\Theta_n$ participating in the indirect optical transitions may be determined from the relation

$$E_g^i = \frac{\varepsilon_{e_n} + \varepsilon_{a_n}}{2}, \qquad k\Theta_n = \frac{\varepsilon_{e_n} - \varepsilon_{a_n}}{2}, \tag{17}$$

where n is the number of phonons. As seen from the analysis, the energies of phonons $k\Theta_1$ and $k\Theta_2$ are respectively equal to 0.01 and 0.52 eV (at $T = 231$ K and $p = 0.25$ GPa). A relatively high energy value $k\Theta_2$ may be ascribed to summing phonon processes or a complicated energy structure of the crystal, when the indirect transitions with some main region are superimposed on the transitions with the other region. For $T = 231$ K and $p = p_{atm}$ the result $k\Theta_1 = 0.008 \pm 0.001$ eV has been obtained. It is easily predicted, since the frequency of phonon vibrations should increase under compression of crystal, while their amplitude should then decrease.

The dependence $E_g^i(T)$ at $p = 0.25$ GPa is displayed in Fig. 14 (see curve 1). At $T = T_c = 279$ K one can see an anomaly, whose character evidences the phase transition from the ferroelectric into paraelectric phase. The temperature coefficients characterizing the shift in E_g^i are $\left(\dfrac{\partial E_g^i}{\partial T}\right)_p^n = -3.7 \times 10^{-4}$ eV K^{-1} for the paraelectric phase and
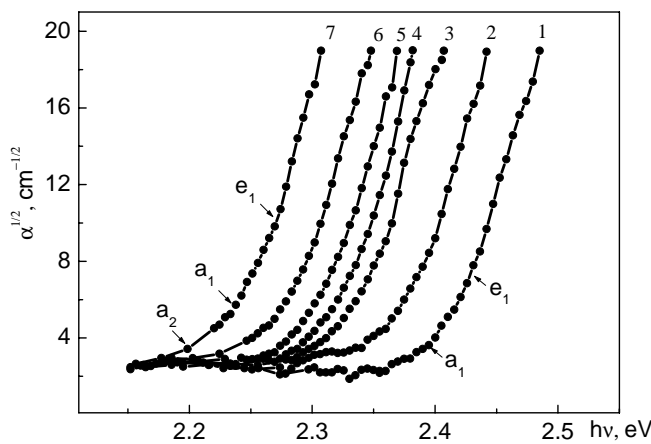
$\left(\dfrac{\partial E_g^i}{\partial T}\right)_p^c = -26.0 \times 10^{-4}$ eV K^{-1} for the ferroelectric phase (close to T_c). The jump of this

coefficient at the phase transition is $\left|\Delta\left(\dfrac{\partial E_g^i}{\partial T}\right)_p\right| = 22.3 \times 10^{-4}$ eV K^{-1}. It is also seen from

Fig. 14 that the break-like anomaly in the $E_g^i(T)$ dependence occurs in the ferroelectric
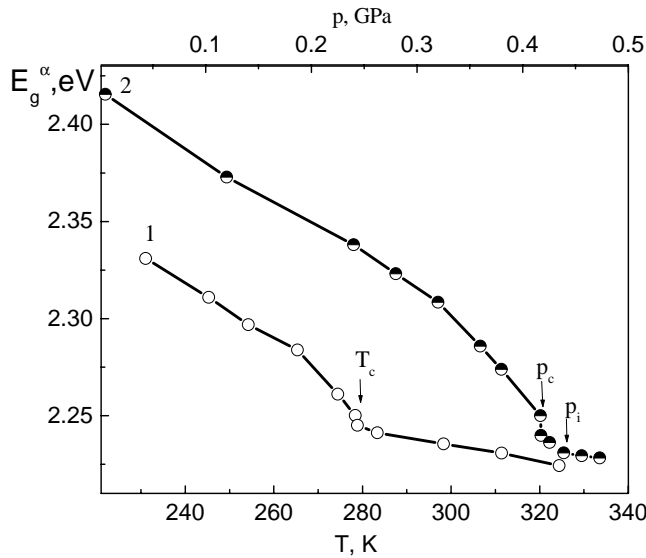
Fig. 14. Dependences of E_g^i on temperature at $p = 0.25$ GPa (curve 1) and on pressure at $T = 244$ K (curve 2).

Fig. 15. Spectral dependences of $\alpha^{1/2}$ at $T = 244$ K and different pressures p: 1 – 0.05, 2 – 0.12, 3 – 0.24, 4 – 0.28, 5 – 0.32, 6 – 0.36 and 7 – 0.42 GPa.

phase near $T = 265\,\text{K}$. Its nature is closely associated with interaction of domain walls with defects of crystalline lattice. The position of this anomaly on the temperature scale varies insignificantly with increasing hydrostatic pressure.

Fig. 15 presents the $\alpha^{\frac{1}{2}}(h\nu)$ dependences at $T = 244\,\text{K}$ and different pressures. All the curves exhibit breaks related to indirect optical transitions. Furthermore, with increasing pressure the dependences shift parallel to each other towards lower energies. The E_g^i values calculated with the aid of Eq. (17) are depicted in Fig. 14 (see curve 2). It is seen that in the vicinities of $p = 0.42$ i $0.45\,\text{GPa}$ the anomalies E_g^i are present, which are caused by the phase transitions occurred at p_c and p_i, respectively. A break is visible in the dependence $E_g^i(p)$ at $p \simeq 0.3\,\text{GPa}$. As with curve 1 for $T = 265\,\text{K}$, it may be ascribed to interaction of defects with P_s. The baric coefficients of E_g^i changes amount to $\left(\dfrac{\partial E_g^i}{\partial p}\right)_T^n = -0.07\,\dfrac{\text{eV}}{\text{GPa}}$ in the paraelectric phase and $\left(\dfrac{\partial E_g^i}{\partial p}\right)_T^c = -0.56\,\dfrac{\text{eV}}{\text{GPa}}$ in the ferroelectric phase near p_c. The jump of this coefficient at the phase transition is equal to $\left|\Delta\left(\dfrac{\partial E_g^i}{\partial p}\right)_T\right| = 0.49\,\dfrac{\text{eV}}{\text{GPa}}$. Inserting the jump values for the corresponding coefficients into Eq. (14), one can obtain $\dfrac{dT_0}{dp} = -220\,\dfrac{\text{K}}{\text{GPa}}$. This coincides with the coefficient dT_0/dp derived in [32] using the studies of p,T-diagram for $(\text{Zn}_{0.05}\text{Sn}_{0.95})_2\text{P}_2\text{S}_6$ crystals.

6. Experimental determination of temperature and baric dependences of the bandgap

As said before, the simplest method for obtaining temperature and baric dependences of E_g in semiconductors is to study the absorption edge. Then the spectral dependences of α might be measured at fixed T and p values. Nonetheless, this method excludes comprehending the effect of dynamic and relaxation processes on the absorption edge, which often accompany phase transitions. Another method for studying $E_g(T,p)$ is based on measuring light transmission at a fixed wavelength within the fundamental absorption region, in the conditions of varying p and T parameters [34]. The method can be explored for narrow enough regions of T and p, thus complicating the studies of crystals with a sequence of phase transitions and crystals exhibiting high coefficients dE_g/dT and dE_g/dp.

The technique for studying $E_g(T,p)$ near the phase transition points proposed in the work [35] includes determining the energy position of the absorption edge and its changes under the influence of T and p. This differs from the techniques mentioned above in that the baric or temperature dependences of energy position of the absorption edge are derived following from the energy of incident photon, for which the optical transmittance t has a fixed magnitude. In this case one compares signals I and I_0 detected by two photoreceivers, which record the radiation transmitted through the diaphragm with the sample under study and without it. The t value should be kept stable as the external factor varies, e.g., through relevant changes in the wavelength of incident light. After amplification, the signals I and I_0 are given at the input of two-coordinate plotter and a computer.

The temperature and baric measurements are performed by means of special optical camera, with the benzine as a medium for transferring high pressures (the refractive index $n=1.7$). The latter considerably decreases the light reflection from the crystal surface. If one neglects the light reflection, the relation between the quantities I, I_0 and t is defined as $I=tI_0$, where all the parameters are dependent on the quantum energy $h\nu$ of incident light. The measurements involve fixing some t value, which corresponds to the appointed value $\alpha=const$ taken from the middle of $0.3 \le \alpha d \le 3.0$ region (with d denoting the sample thickness). The value $\alpha=const$ specifies the slope of $I=I(I_0)$ dependence (see Fig. 16).
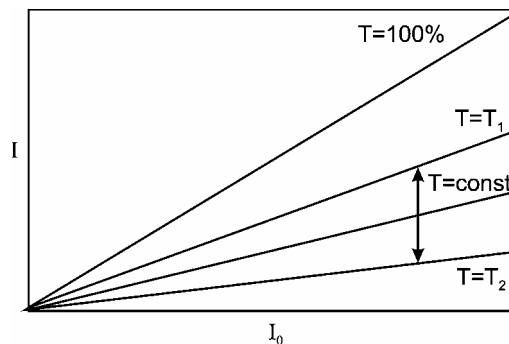

Fig. 16. Dependences $I(I_0)$ at fixed α values [35].

External actions change transmittance t to the values t_1 or t_2. While changing the incident quantum energy with monochromator, one reaches decrease or increase in the optical transmittances (t_1 or t_2) to the value $t=const$. Recording $h\nu$ for the given T and p values, one obtains the dependence $E_g^\alpha(T,p)$ characterizing the temperature or baric E_g changes. The error $\Delta E_g^\alpha(T,p)$ related with the measurements is of the order of $\pm 5 \times 10^{-4}$ eV. Recording process for the $E_g^\alpha(T,p)$ dependence might easily be automated,

using a computer and a step motor for changing the wavelength of the light emergent from monochromator.

The results of the studies carried out for $Sn_2P_2Se_6$, SbSJ and $Sn_2P_2S_6$ are summarized in Fig. 17. They agree excellently with the data of other measurements. From Fig. 17 (curves 1 and 3) one can see breaks in the $E_g(T)$ dependences taking place at T_i and T_0 for $Sn_2P_2Se_6$ and $Sn_2P_2S_6$, respectively. They are explained by the second-order phase transitions. On the other hand, the jumps present in the $E_g^\alpha(T)$ dependences for
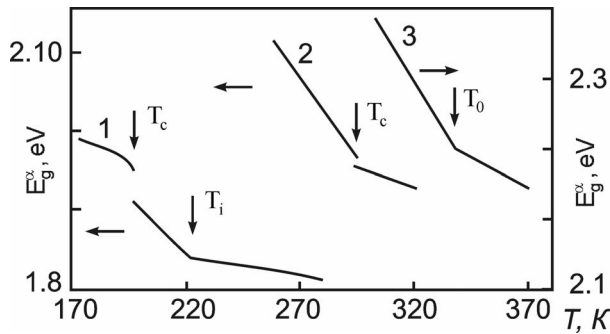
Fig. 17. Temperature dependences of E_g^α for: $Sn_2P_2Se_6$ (1), SbSJ (2) and $Sn_2P_2S_6$ (3) at $p = p_{atm}$ [35].

$Sn_2P_2Se_6$ (curve 1) and SbSJ (curve 2) are related to the phase transition of first order located at T_c. The method for studying $E_g^\alpha(T, p)$ described above also allows judging the shape of the absorption edge and determining the parameters governing the Urbach rule. This may be done following from the measurements of iso-absorption curves.
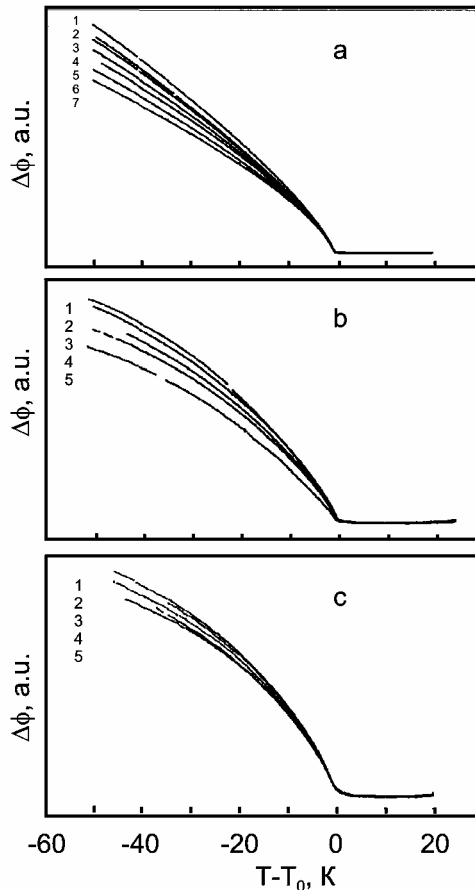
7. Optical birefringence of $Sn_2P_2\left(Se_xS_{1-x}\right)_6$ crystals under high pressure

Anomalous part of optical birefringence for proper ferroelectrics in the region of weak fluctuation corrections is proportional to the square of spontaneous polarization ($\Delta n \sim P_s^2 \sim \tau^{2\beta_{cr}}$, with $\tau = (T - T_0)/T_0$ denoting the reduced temperature). Besides, the first temperature derivative of Δn should be proportional to the anomalous part of specific heat capacity ($d\Delta n(T)/dT \sim \Delta C_p \sim \tau^{-\alpha_{cr}}$) in the overall region of T. These facts enable determining the critical indices and the Landau-Ginzburg coefficients on the basis of experimental dependences of $\Delta n(T)$.

The temperature dependence of the birefringence for $Sn_2P_2(Se_xS_{1-x})_6$ crystals with $x = 0$, 0.1 and 0.2 have been studied in the work [36] under different hydrostatic pressures. Measurements of $\Delta n(T)$ have been implemented by means of Senarmont technique for the light wavelength of $\lambda = 0.6328\,\mu m$. The experiment has dealt with changes in the orientation angle $\Delta\varphi$ of analyzer, which is proportional to Δn variations. Single crystalline samples under test have been prepared in the shape of plates of (001) and (010) cuts and had the linear dimensions $1 \times 3 \times 3$ mm^3. The β_{cr} parameter

has been determined from the slopes of $\Delta\varphi \sim f(\tau)$ dependences plotted on logarithmic scale, using the relationship $\ln\Delta\varphi \sim 2\beta_{cr} \ln(\tau)$.

It is seen from Fig. 18 that the dependences $\Delta\varphi(T)$ manifest the anomalies characteristic for the phase transitions of second order. Increasing hydrostatic pressure causes the anomalies to shift towards lower temperatures, with simultaneous decrease of $\Delta\varphi$ values in the ferroelectric phase. The anomalous part of the birefringence obeys the relation $d\Delta\varphi/dT \sim \tau^{-\alpha_{cr}}$, with $\alpha_{cr} = 0.5$. When the temperature changes, the α_{cr} value increases near T_0 and approaches $\alpha_{cr} = -1.5$, typically for the case of influence of defects on the critical phenomena [37]. Accounting for the contribution of static defects, one can write $d\Delta\varphi/dT \sim A\tau^{-0.5} + B\tau^{-1.5}$, where the A coefficient describes the fluctuation contribution and B that of defects. Variation of chemical content of $Sn_2P_2(Se_xS_{1-x})_6$ crystals from $x = 0$ to $x = 0.2$ gives rise to enlarged defect contribution to the critical anomaly, so that the corresponding ratio varies from $B/A = 10^{-3}$ up to 10^{-2}.
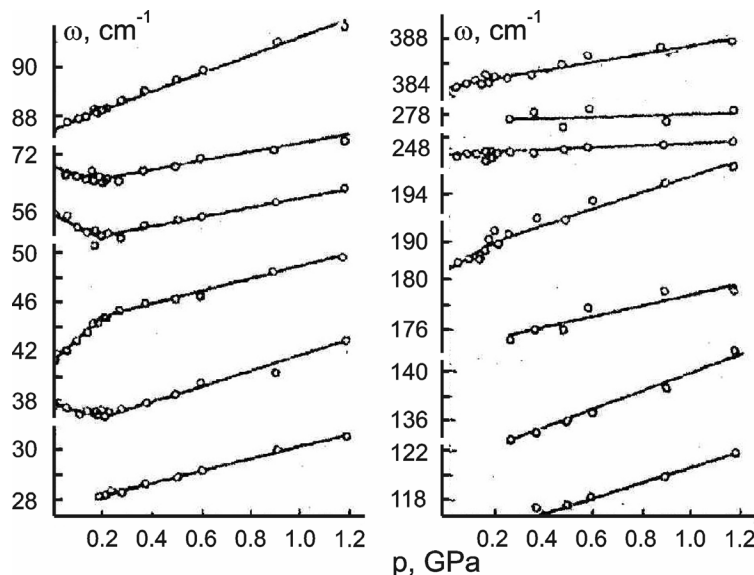
It is demonstrated experimentally that, under the atmospheric pressure, the increase of Se content in the solid solutions $Sn_2P_2(Se_xS_{1-x})_6$ decreases β_{cr} from 0.41 (for $x = 0$) to 0.32 (for $x = 0.2$). This is readily explained by approaching the Lifshitz point. Increasing hydrostatic pressure leads to decrease in β_{cr}, too. Just at the Lifshitz point, we obtain the β_{cr} value correlated with that derived from the studies ε, P_s and χ_V. We should stress, however, that some of the $\Delta\varphi(T)$ measurements performed for the mentioned crystals at

Fig. 18. Temperature dependences of anomalous part of the birefringence for the $Sn_2P_2(Se_xS_{1-x})_6$ crystals at different hydrostatic pressures p, GPa :
(a) 1 − 0, 2 − 0.017, 3 − 0.051, 4 − 0.07, 5 − 0.102, 6 − 0.129, 7 − 0.164;
(b) 1 − 0.10, 2 − 0.0135, 3 − 0.0405, 4 − 0.0740, 5 − 0.112;
(c) 1 − 0.003, 2 − 0.0065, 3 − 0.0195, 4 − 0.0300, 5 − 0.0600.
The concentration x is $x = 0$ (a), $x = 0.1$ (b) and $x = 0.2$ mol. % (c).

different pressures have given the value $\beta_{cr} = 0.33$ at the Lifshitz point (see [38]). This coincides with the result calculated theoretically in the mean-field approximation for the universality class UL [39]. On the basis of $\Delta n(T)$ data for different pressures one concludes that the coefficient β at P_s^4 in the expansion of thermodynamic potential in a power series of the order parameter P_s is positive and increases with approaching the Lifshitz point on the p,T-diagram.

8. Vibrational spectra of $Sn_2P_2S_6$ under hydrostatic pressure

Dependences of frequencies of internal and external modes on the interatomic distances provide important information on anharmonicity of the lattice vibrations. Different types of vibrations are peculiar for $Sn_2P_2S_6$. These are external vibrations of $[P_2S_6]^{4-}$ complexes (located below $150\,cm^{-1}$), deformation vibrations S-P-S and "bending" modes, e.g., tilts of PS_3 groups belonging to $[P_2S_6]^{4-}$ anions (from 150 to $260\,cm^{-1}$), vibrations of P-P bonds (located at $381\,cm^{-1}$) and internal valence P-S modes ($560 - 583\,cm^{-1}$) [28].

In order to study baric dependences of the Raman spectra of $Sn_2P_2S_6$, the authors [42] have used a krypton laser $(\lambda = 641.1\,nm)$ and a spectrometer DFS-24. The corresponding results are depicted in Fig. 19. It is seen that a portion of external vibrations in the ferroelectric phase possess "negative" pressure dependences, whereas in the paraelectric phase these dependences are "positive" for the all modes. The baric dependences of some frequencies have breaks near the Lifshitz point (at $p = 0.19\,GPa$).

Under external pressure, the internal modes of $[P_2S_6]^{4-}$ anions do not change notably near p_c (except for the "bending" modes), thus testifying that

**Fig. 19.** Baric dependences of the frequencies found in the Raman spectra of $Sn_2P_2S_6$ crystals [40].

the structural changes in the crystal taking place at the phase transition are due to Sn-S bonds. If $T = 296\,\mathrm{K}$ and $p = 0.18\,\mathrm{GPa}$, the transition still remains continuous and no jumps are seen in the $\omega(p)$ dependences.

The Gruneisen parameter Γ_i for some of the external modes is negative, in accordance with the fact of elongation of Sn-S bonds under external pressure. A negative Γ_i value agrees with the data of experimental studies of linear expansion coefficient α for the $Sn_2P_2S_6$ crystals [41]. According to those studies, the parameter α near T_0 is negative. The baric studies of the Raman spectra also confirm the known mechanism of the phase transition in $Sn_2P_2S_6$ as a displacement-type one. This conclusion may be drawn because ferroelectric transformations into paraelectric phase of the order-disorder type should have been accompanied by increasing damping of the external or internal valence vibrations. However, the analysis of linewidth of those vibrations has not revealed any changes in the region of pressures higher than the critical one. This proves the absence of structural disordering in the paraelectric phase of $Sn_2P_2S_6$.

A strong nonequivalence of interatomic forces has been found for the $Sn_2P_2S_6$ crystals. As a consequence, the relative pressure-induced shift of the frequencies,

$$\gamma_i = \frac{1}{\omega_1}\frac{d\omega_1}{dp}, \qquad (18)$$

can increase one or two orders of magnitude if we pass from the internal to external vibrations. This is associated with different pressure sensitivities of weak inter-molecular and strong intra-molecular bonds. Fig. 20 presents the dependence $\ln\gamma_i(\ln\omega)$, which confirms the above conclusion. Indeed, the γ_i value for different modes differs by almost three orders of magnitude. Fig. 20 also testifies that the dependences $\ln\gamma_i(\ln\omega)$ include two linear regions. The line with a less slope $\left(\gamma_i \sim \omega^{-0.8}\right)$ corresponds to the external modes related to Sn-S bonds, while the line with a steeper slope ($\gamma_i \sim \omega^{-1.8}$) to the internal vibrations.
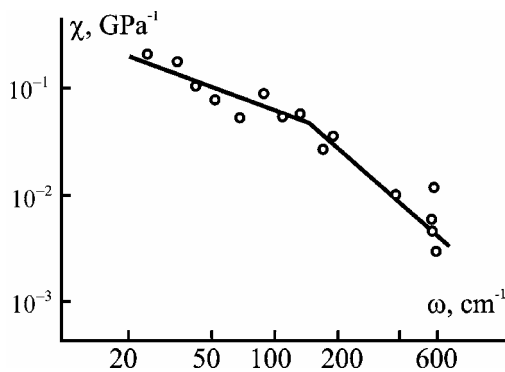

Fig. 20. Frequency dependence of the coefficient of relative frequency shift for the vibrations detected in the paraelectric phase of $Sn_2P_2S_6$ crystals at $p = 0.2\,\mathrm{GPa}$.

High pressures affect appreciably Sn-S bonds and hardly perturb covalent P-P and P-S bonds. The two points in Fig. 20 located below the line $\gamma_i \sim \omega^{-1.8}$ correspond to deformation S-P-S vibrations with the frequencies of 248 and $278 \, \text{cm}^{-1}$. Insignificant influence of pressure on those vibrations is explained by small changes in the angles of S-P-S bonds available in the structural PS_3 groups. The internal vibrations of anions manifested through bending of PS_3 groups as a single whole with respect to the P-P bonds (the modes at 175 and $190 \, \text{cm}^{-1}$) appear to be more sensitive to changing pressure, if compare with the deformation S-P-S vibrations (the modes located at 248 and $278 \, \text{cm}^{-1}$). This is evidenced by large γ_i values for these modes. A break in the dependences $\ln \gamma_i (\ln \omega)$ corresponds to the frequency limit $(\omega = 150 \, \text{cm}^{-1})$ that divides the vibrations into external and internal ones. The latter limit has also been derived independently from comparison of the data for isomorphous ionic substitutions in the crystals under study. As a result, the interatomic interaction forces in $Sn_2P_2S_6$ are essentially inequivalent.

The authors [41] have also shown that a notable pressure-induced decrease for the "bending" modes of the anions, which are the lowest-frequency modes among the internal ones, should lead to their link with the external lattice vibrations. Analogous effect has been observed in the solid solutions of $Sn_2P_2(Se_xS_{1-x})_6$ under $S \rightarrow Se$ substitution, though it is absent in $(Pb_ySn_{1-y})_2P_2(Se_xS_{1-x})_6$ crystals under $Sn \rightarrow Pb$ substitution.

9. Frequency converters for the coherent electromagnetic radiation

A shift of the phase transition temperature of ferroelectric under external pressure and, as a consequence, change in the soft-mode frequency have been used in Ref. [42] for converting coherent long-wavelength infrared radiation from the region of $200 - 1000 \, \mu\text{m}$, whose frequency is continuously changed, into a higher-frequency radiation. With this purpose, the coherent long-wavelength infrared radiation under converting excites the lattice vibrations in crystal and the crystal is irradiated by additional laser source. As a result, we have parametric generation of radiation at the sum (anti-Stokes) and difference (Stokes) frequencies. Within the method, one uses a crystal
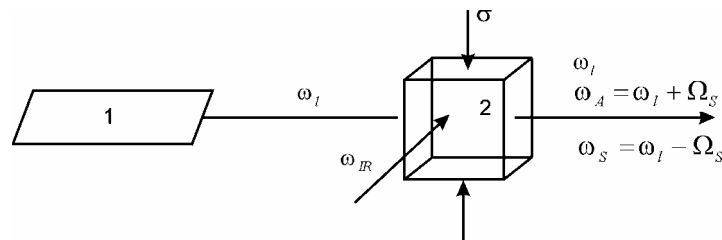
Fig. 21. Scheme of the device for continuous frequency conversion [42].

with the structural phase transition, in which soft-lattice vibration can be excited. The crystal is compressed along the direction of polarization for this vibration at a fixed temperature. This allows efficient conversion of the coherent long-wavelength infrared radiation and continuous frequency tuning. Among the advantages of the method we note only the absence of magnetic fields and liquid-helium temperatures, as well as a simple construction of the corresponding device.

A scheme of such a frequency-converting device is shown in Fig. 21. We use the following notation on that scheme: 1 – laser, 2 – crystal, ω_{IR} – the frequency of long-wave infrared radiation under conversion, ω_l – the laser radiation frequency, $\omega_A = (\omega_l + \Omega_S)$ – the sum anti-Stokes frequency, $\omega_S = (\omega_l - \Omega_S)$ – the difference Stokes frequency, Ω_S – the frequency of soft-mode lattice vibration, and σ – the compression stress applied to the crystal.

According to the scheme described above, the technique for continuous conversion of the frequency of coherent long-wavelength infrared radiation is based on Raman scattering of laser radiation with the frequency ω_l at the mixed photon-phonon excitations in crystals (polaritons), which have the frequency ω_P. In general, this scattering formally represents a superposition of two effects: (1) the parametric generation of the sum ($\omega_+ = (\omega_l + \omega_P)$) and difference ($\omega_- = (\omega_l - \omega_P)$) frequencies, involving a photon constituent of the polariton, and (2) the Raman scattering itself, involving a phonon constituent of the polariton. Then the radiation with the frequency $\omega_l + \omega_P$ corresponds to the anti-Stokes component, while the radiation with the frequency $\omega_l - \omega_P$ to the Stokes component.

The coherent long-wavelength infrared radiation with the frequency $\omega_{IR} = \omega_P$ that falls upon the crystal gives rise to additional excitation of polaritons. It is this point that enables one to increase significantly the radiation intensity at the Stokes and anti-Stokes frequencies, when compare with the ordinary (spontaneous) Raman scattering. The radiation intensity at the Stokes and anti-Stokes frequencies is unambiguously defined by the intensity of coherent long-wavelength infrared radiation, i.e. we deal with an up-frequency conversion of this long-wavelength infrared radiation.

The crystals employed in frame of the above technique should efficiently scatter laser radiation and, moreover, reveal a soft mode, which must be active simultaneously in the infrared absorption spectra and the Raman spectra. Furthermore, there should be a possibility for converting the soft-mode frequency by means of application of stresses σ, while the operating temperature region, which depends on the Curie point of crystal, should be convenient enough. At last, the soft mode should exhibit a large cross-section of the scattering and a longitudinal-transverse splitting proportional to the photon-phonon interaction.

The crystals $Sn_2P_2S_6$ meet all of those demands. Therefore the technique described above can be carried out, provided that the soft lattice mode is excited by the coherent long-wavelength infrared radiation ω_{IR} in the crystallographic direction [001] and the radiation of He-Ne laser ($\lambda = 0.63\,\mu$m)propagating along the [010] direction is scattered by the excited lattice vibration. At the room temperature the soft-mode frequency for the $Sn_2P_2S_6$ crystal can be varied from 30 to $10\,cm^{-1}$, using the uniaxial pressure $0-400\,kg\,cm^{-2}$ applied in the direction [101]. This would allow converting continuously the radiation from the region of $330-1000\,\mu$m into the radiation located near $\lambda = 0.63\,\mu$m.

10. Conclusions

The studies of ferroelectrics-semiconductors of $A_2^{IV}B_2^{V}C_6^{VI}$ group under the influence of hydrostatic pressure have shown that their absorption edge in its high-energy part obeys the Urbach rule both in the paraelectric and ferroelectric phases. If the absorption coefficients are small enough, the absorption edge is formed by the indirect optical transitions. A violation of the Urbach rule occurs inside the incommensurate phase of those crystals. The baric and temperature coefficients of the bandgap changes are negative for all of the phases. The E_g anomalies near the phase transitions testify that the phase transition lines $T_0(p)$ and $T_i(p)$ available on the p,T-diagram represent the lines of second-order phase transitions, whereas the line $T_c(p)$ is that of the first-order transitions.

Near the Lifshitz point, the jumps of the first derivatives $\left(\dfrac{\partial E_g}{\partial p}\right)_T$ and $\left(\dfrac{\partial E_g}{\partial T}\right)_p$ on the phase transition line $T_0(p)$ are replaced by the jumps ΔE_g on the phase transition line $T_c(p)$. The E_g anomaly occurred at the phase transition is shifted by the pressure towards the lower temperatures. The latter fact confirms the earlier results of dielectric measurements. They have revealed that the phase transition in the ferroelectrics of $A_2^{IV}B_2^{V}C_6^{VI}$ family may be attributed to displacement-type transitions. It follows from the temperature and baric dependences of the E_g parameter that the electron-phonon interaction plays a major part in the temperature changes of the bandgap, like in the most of semiconducting crystals.

The experimental values of critical indices referred to the order parameter and the heat capacity determined from the baric measurements of optical birefringence in $Sn_2P_2S_6$ crystals and the solid solutions $Sn_2P_2(Se_xS_{1-x})_6$ are close to those predicted by the theory for the Lifshitz point. In particular, a baric increase in the β coefficient

entering the term P_s^4 in the expansion of thermodynamic potential, which follows from the birefringence data, is typical for the vicinity of the Lifshitz point.

The relative shift in the frequencies obtained in the Raman spectra under external pressure shows that different interatomic bonds are notably inequivalent and the vibrations characteristic for $Sn_2P_2S_6$ might be divided into internal and external ones. Moreover, it follows from the baric studies of the Raman spectra that the frequencies observed for the paraelectric phase have positive baric coefficients, unlike the ferroelectric region where they are negative. The structural transformation of $Sn_2P_2S_6$ in the course of phase transition is mainly due to Sn-S bonds. At the same time, the absence of jumps for the frequencies found in the Raman spectra at $p = 0.12\,GPa$ and $T = 290\,K$ confirms the conclusion about a continuous phase transition occurring at T_0.

The effects of baric shift of the phase transition temperature for the $Sn_2P_2S_6$ crystals and, correspondingly, the soft-mode frequency shift offer the idea of continuous conversion of frequency of coherent light. It is experimentally implemented on the example of converting the two-wave infrared radiation from the region of $200\text{-}1000\,\mu$m into higher-frequency region, not far from $\lambda = 0.63\,мм$.

References

1. Carpentier G and Nitsche R, 1974. Ferroelectricity in $Sn_2P_2S_6$. Mat. Res. Bull. **9**: 1097–1103.

2. Ditmar G and Shafer H, 1974. Die Structur des Di-Linn-Hexathiohipodiphosphats $Sn_2P_2S_6$. Z. Naturforsch. **298**: 312–317.

3. Nitsche R and Wild R, 1974. Crystal growth of metal-phosphorus-sulfur compounds by vapor transport. Mat. Res. Bull. **9**: 419–424.

4. Carpentier C D and Nitsche R, 1974. Vapour growth and crystal data of thio(seleno)-hypodiphosphate $Sn_2P_2S_6$, $Sn_2P_2Se_6$, $Pb_2P_2S_6$, $Pb_2P_2Se_6$ and their mixed crystals. Mat. Res. Bull. **9**: 401–410.

5. Klingen W, Ott R and Hahn H, 1973. Uber die Darstellung und Eigenschaften von Hexathio-und Hexaselenohypodiphosphaten. Z. Anorg. Allg. Chem. **396**: 271–278.

6. Vysochanskii Yu M and Slivka V Yu, Ferroelectrics of $Sn_2P_2S_6$ family: Properties in the vicinity of Lifshitz: Lvov: Nauchnoye Izdaniye, 1994. 264 p.

7. Slivka A G, Gerzanich E I, Tyagur Yu I and Yatskovich I I, 1986. Phase diagram of ferroelectric solid solutions $Sn_2P_2(Se_xS_{1-x})_6$. Ukr. Fiz. Zhurn. **31**: 1372–1374.

8. Shusta V S, Gerzanich E I, Slivka A G, Guranich P P and Bobela V A, 1993. Phase transitions and physical properties of $(Pb_ySn_{1-y})P_2S_6$ crystals at high hydrostatic pressure. Ferroelectrics. **145**: 61–71.

9. Guranich P P, Gerzanich E I, Slivka A G, Shusta V S and Bobela V A, 1992. Phase p,T,x-diagram and peculiarities of physical properties of $(Pb_ySn_{1-y})P_2Se_6$ crystals with on incommensurate phase. Ferroelectrics. **132**: 173–183.

10. Slivka A G, Gerzanich E I, Shusta V S and Guranich P P, 1999. Effect of isomorphous substitution and external hydrostatic pressure on the fundamental optical absorption edge of $Sn(Pb)_2P_2 S(Se)_6$ crystals. Izv. Vuzov., Ser. Fiz. **9**: 23–28.

11. Buturlakin A P, Gerzanich E I, Tyagur Yu I, Gurzan M I and Chepur D V, 1980. Influence of high hydrostatic pressure on the optical properties of ferroelectric-semiconductor $Sn_2P_2S_6$. Proceeding of III Republic Seminar «High Pressure and Properties of Materials», Kyiv, Naukova Dumka. **2**: 29–32.

12. Gerzanich E I, Buturlakin A P, Tyagur Yu I, Gurzan M I and Chepur D V, 1980. Studies of semiconducting properties of ferroelectric crystals $Sn_2P_2S_6$ along their p,T-diagram. Izv. Vuzov, Ser. Fiz. **23**: 93–96.

13. Slivka A G, Gerzanich E I, Studenyak I P, Kovach D Sh and Seykovskaya L A, 1987. Absorption edge of $Sn_2P_2(Se_{0.30}S_{0.70})_6$ crystals and its dependence on temperature and hydrostatic pressure. Ukr. Fiz. Zhurn. **32**: 1819–1822.

14. Gerzanich E I, Slivka A G, Guranich P P and Shusta V S, 1992. Influence of anionic and cationic substitutions on the fundamental absorption in $Sn_2P_2S_6$ crystals. Republican Scientific Technical Collection «Materials for Optoelectronics», Kyiv, Tekhnika. **1**: 31–38.

15. Shusta V S, Gerzanich E I, Slivka A G, Guranich P P and Bobela V A, 1992. Urbach-like behaviour of the absorption edge of ferroelectric crystals $(Pb_ySn_{1-y})_2P_2S_6$. Ukr. Fiz. Zhurn. **37**: 561–565.

16. Gerzanich E I, Guranich P P, Slivka A G, Shusta V S, Gurzan M I and Kedyulich V M, 1997. Baric dependence of fundamental absorption edge in the course of phase transitions in the proper ferroelectrics of $Sn_2P_2S_6$ type. Izv. Vuzov., Ser. Fiz. **8**: 82–85.

17. Studenyak I P, Mitrovcij V V, Kovach Gy Sh, Mykajlo O A, Gurzan M I and Vysochanskii Yu M, 2001. Temperature Variation of optical Absorption Edge in $Sn_2P_2S_6$ and SnP_2S_6 crystals. Ferroelectrics. **254**: 295–310.

18. Vlokh R O, Grabar A A and Kityk I V, 1991. Electronic structure of single crystals $Sn_2P_2S_6$. Izv. FN SSSR., Ser. Neorg. Mat. **27**: 2052–2054.

19. Yakubovskii M A, Zametin V I, Rabkin M M and Fesenko E G, 1980. Absorption edge of calcium titanate. Fiz. Tverd. Tela. **22**: 3523–3528.

20. Sumi H and Toyozawa Y, 1971. Urbach-Martienssen rule and exciton trapped monentarily by lattice vibrations. J. Phys. Soc. Jap. **31**: 342–358.

21. Skettrup T, 1978. Urbach's rule derived from thermal fluctuations in the bang-gap energy. Phys. Rev. B. **18**: 2622–2631.

22. Glebov L B and Tolstoy N N, 1975. Influence of temperature on the fundamental absorption spectrum of soda-lime glass. Fiz. Khim. Stekla. 1: 239–242.

23. Cody G D, Tiedje T, Abeles B. Brooks B and Goldstein Y, 1981. Disordering and the Optical-Absorption Edge of Hydrogenated Amorphous Silicon. Phys. Rev. Lett. **47**: 1480–1483.

24. Zametin V I, Yakubovskii M A and Rabkin L I, 1979. Anomalies of the absorption edge caused by phase transitions. Fiz. Tverd. Tela. **21**: 491–498.

25. Vlokh O G, Polovinko I I and Sveleba S A, 1988. Optical absorption of incommensurate crystals $(N(CH_3)_4)_2CuCl_4$. Opt. Spektr. **65**: 1272–1275.

26. Strukov B A and Levanyuk A P, Physical basics of ferroelectric properties of crystals: Moscow: Nauka, 1983.

27. Parsamyan T K, Khasanov S S, Shehtman V M, Vysochanskii Yu M and Slivka V Yu, 1985. Incommensurate phase in proper ferroelectrics $Sn_2P_2Se_6$. Fiz. Tverd. Tela. **27**: 3327–3331.

28. Vysochanskii Yu M, Slivka V Yu, Voroshylov Yu V and Gurzan M I, 1979. Model of phase transition in ferroelectric-semiconductor $Sn_2P_2S_6$ and its lattice dynamics. Fiz. Tverd. Tela. **21**: 2402–2408.

29. Slivka A G, 2001. Absorption edge of $Sn(Pb)_2P_2S(Se)_6$ crystals under hydrostatic pressure. Ukr. J. Phys. Opt. **2**: 171–178.

30. Slivka A G, Gerzanich E I, Tyagur Yu I and Korda N F, 1988. Splitting of phase transition in the ferroelectric solid solutions $Sn_2P_2(Se_xS_{1-x})_6$ under high pressure. Izv. Vuzov, Ser. Fiz. **2**: 28–32.

31. Guranich P P, Gerzanich E I, Shusta V S, Slivka A G, 1988. Phase p,T,x-diagram of ferroelectric crystals $(Pb_ySn_{1-y})P_2Se_6$ with incommensurate phase. Fiz. Tverd. Tela. **30**: 1189–1191.

32. Shusta V S, Tovt V V, Slivka A G, Guranich P P, Gerzanich E I and Kuritsa I Y, 2005. Temperature and pressure effect on absorption edge in $(Zn_{0.05}Sn_{0.95})_2P_2S_6$ crystal. Ferroelectrics. **317**: 83–87.

33. Maclean T P, 1960. The absorption edge spectrum of semiconductors. Progress in Semiconductors. **5**: 53–102.

34. Gerzanich E I, Bryzgalov I A, Rakcheev A D and Lyahovitskaya V A, 1968. Optical constants of single crystals SbSI. Kristallogr. **13**: 898–900.

35. Shusta V S, Guranich P P, Gerzanich O I and Slivka O G. Patent No. 33019 (Ukraine). Express method for studying energetic structure of solids in the region of phase transitions. Bull. No. 5, 15.05.2003.

36. Guranich P P, Kabal R V, Slivka A G and Gerzanich E I, 2001. Pressure behaviour of the birefringence in $Sn_2P_2(Se_xS_{1-x})_6$ crystals in the vicinity of the Lifshitz point. Ukr. J. Phys. Opt. **2**: 179–181.

37. Isaverdiyev A A, Levanyuk A P, Lebedev N I, Sigov A S, 1989. Influence of point defects on the properties of ferroelectrics with a single axis of spontaneous polarization near the Lifshitz point. Fiz. Tverd. Tela. **31**: 272–274.

38. Folk R and Moser G, 1993. Lifshitz point in uniaxial ferroelectrics. Phys. Rev. B. **47**: 13992–13997.

39. Hasser I, Abdel-Hady A and Folk R, 1997. Specific-heat amplitude ratio near a Lifshitz point. Phys. Rev. B.**56**: 154–160.

40. Grabar A A, Vysochanskii Yu M, Melnik N N, Subbotin S I, Panfilov V V and Slivka V Yu, 1984. Influence of hydrostatic pressure on the vibrational spectra of $Sn_2P_2S_6$ ferroelectrics. Fiz. Tverd. Tela. **26**: 65–68.

41. Major M M, Koperlyos B M, Savchenko B A, Gurzan M I, Morozova O V and Korda N F, 1983. Heat capacity and linear expansion of $Sn_2P_2(Se_xS_{1-x})_6$ crystals. Fiz. Tverd. Tela. **25**: 214–223.

42. USSR Inventors Certificate No. 1329420. Vysochanskii Yu M, Slivka V Yu, Furtsev V G, Grabar A A and Chepur D V. Published 05.07.1982. Method for the conversion of coherent long-wave infrared radiation with increasing frequency.